Enhanced reaction kinetics and reactive mixing scale dynamics in mixing fronts under shear flow for arbitrary Damköhler numbers

Aditya Bandopadhyay[a], Tanguy Le Borgne[a], Yves Méheust[a], Marco Dentz[b]

[a] *Université de Rennes 1, CNRS, Géosciences Rennes UMR 6118, 35042 Rennes, France*
[b] *Spanish National Research Council (IDAEA-CSIC), E-08034 Barcelona, Spain*

Abstract

Mixing fronts, where fluids of different chemical compositions mix with each other, are known to represent hotspots of chemical reaction in hydrological systems. These fronts are typically subjected to velocity gradients, ranging from the pore scale due to no slip boundary conditions at fluid solid interfaces, to the catchment scale due to permeability variations and complex geometry of the Darcy velocity streamlines. A common trait of these processes is that the mixing interface is strained by shear. Depending on the Péclet number Pe, which represents the ratio of the characteristic diffusion time to the characteristic shear time, and the Damköhler number Da, which represents the ratio of the characteristic diffusion time to the characteristic reaction time, the local reaction rates can be strongly impacted by the dynamics of the mixing interface. So far, this impact has been characterized mostly either in kinetics-limited or in mixing-limited conditions, that is, for either low or high Da. Here the coupling of shear flow and chemical reactivity is investigated for arbitrary Damköhler numbers, for a bimolecular reaction and an initial interface with separated reactants. Approximate analytical expressions for the global production rate and reactive mixing scale are derived based on a reactive lamella approach that allows for a general coupling between stretching enhanced mixing and chemical reactions. While for $\mathsf{Pe} < \mathsf{Da}$, reaction kinetics and stretching effects are decoupled, a scenario which we name "weak stretching", for $\mathsf{Pe} > \mathsf{Da}$, we uncover a "strong stretching" scenario where new scaling laws emerge from the interplay between reaction kinetics, diffusion, and stretching. The analytical results are validated against numerical simulations. These findings shed light on the effect of flow heterogeneity on the enhancement of chemical reaction and the creation of spatially localized hotspots of reactivity for a broad range of systems ranging from kinetic limited to mixing limited situations.

Keywords: Reactive front, mixing, arbitrary Damköhler number, shear flow, reaction width

1. Introduction

Reaction fronts where two reactive fluids displace one another play an important role in a range of processes, including contaminant plume transport and reaction, soil and aquifer remediation, CO_2 sequestration

Email address: aditya.bandopadhyay@univ-rennes1.fr (Aditya Bandopadhyay)

and the development of hotspots of reaction in mixing zones [1, 2, 3, 4, 5, 6, 7]. Mixing of reactants by heterogeneous flows leads to the formation of geometrically-complex fronts, at which chemical reactions occur [8, 9, 10, 11, 12, 13, 14, 15, 16, 17, 18], Such fronts are subjected to fluid deformation which increases the surface available for diffusive mass transfer thereby enhancing effective reaction rates [19, 20, 21, 22, 23, 24, 25].

The dynamics of reactive mixing systems has been widely studied in the absence of velocity gradients. Galfi and Racz [26] and Larralde et al. [27] studied diffusion coupled to the reversible bimolecular reaction $A + B \rightleftharpoons C$ for the case of initially well separated reactants at different bulk concentrations. The mathematical insights obtained through the long-time asymptotics are that the mass of product formed, m_c, grows as $m_c \sim t^{1/2}$, which is expected from the diffusive flux across the interface, while the width of the reaction front s_r grows as $s_r \sim t^{1/6}$, due to the balance between the diffusive growth and the reactive consumption. Taitelbaum et al. [28] had studied the initial time dynamics of such reactive fronts for a bimolecular reaction and showed that the rate of production of the product grows as $t^{1/2}$ as opposed to the asymptotic long-time limit t^{-1}. For a similar reactive front, Arshadi and Rajaram [29] found by means of regular perturbation analysis that the growth rate of the total product mass behaves as $dm_c/dt \sim t^{1/2}$ at short times while at larger times it evolves as $dm_c/dt \sim t^{-1/2}$; the transition time between the two regimes is shown to depend on the rate constant and diffusion coefficient. Similar observations of the kinetic diffusive regimes were observed in the work by Chopard et al. [30] who focused on quantification of the influence of the reversible reaction in comparison to the forward reaction, with an emphasis on the formalism of cellular automata. This problem was also addressed through a mean-field formalism for species with different reactivities by Sinder and Pelleg [31] with the product formed being immobile. Results for reactive fronts for the annihilation reaction ($A + B \rightarrow \Phi$) were obtained through probabilistic cellular automata for a 1D case [32] where it was shown that the reaction width grows as $w \sim t^{1/4}$. The validity of the analytical results were then investigated for higher dimensions by Howard and Crowdy [33]. They found that the characteristic time of the crossover between the initial time irreversible and the long time reversible behaviour depends on the inverse of the Damköhler number based on the reversible kinetics rate constant. Several other works relate to reaction-diffusion waves in autocatalytic systems ($A + nB \rightarrow (n + 1)B$) [34] where the front propagation velocity is obtained analytically in the long time limit. Merkin et al. [35, 36, 37] also developed solutions for the situations of well stirred mixtures and low catalyst concentrations where the catalyzer decays in time through a parallel reaction ($B \rightarrow C$). Taitelbaum [38] studied the influence of initial conditions and fluctuations on the segregation and patterns formed by such bimolecular systems. Taitelbaum et al. [39] studied the influence of bias on the reaction kinetics of bimolecular reactive fronts. This study was motivated by the observations of Koo and Kopelman [40] that the reaction kinetics of injected fronts, i.e. without a stationary front, do not follow the analytical predictions of Galfi and Racz [26]. Park et al. [41] performed experiments to prevent the advective motion of such injections and showed that the analytical predictions of the scalings of the reactive fronts agrees well with experimental observations of

copper ion-complex formation reactions. Havlin et al. [42] and Bazant and Stone [43] have also considered the scenario of diffusion-reaction kinetics for a system with one static component (for example, a solid porous catalyst). Through analytical solutions, Taitelbaum and Koza [44] have shown that the reaction fronts for initially well separated reactants may move forward or backward depending upon the relative diffusivity of the two species reacting species (see also [45, 46]). Benson et al. [47] have analyzed an annihilation reaction between two reactants to study the mixing density. Sinder and Pelleg [48] analyzed the reactive boundary layer between a two species reversible reaction system ($A \leftrightarrow B$) by means of a singular perturbation analysis for fast reactions, i.e where the characteristic reaction time is much smaller than the characteristic diffusion time. On similar lines, Sinder and Pelleg [49] analyzed a system with two competing reactions and found analogous irreversible initial regimes followed by a crossover regime depending on the reaction kinetics. It is shown that the reversible time regime encompasses two distinct reversible and irreversible zones near the reaction front. When velocity gradients exist in a fluid flow, transported reactive mixtures are submitted to repeated stretching actions that lead to the formation of elongated lamellar structures. The latter are known to promote mixing and enhance reaction rates [19, 50, 51, 52, 53, 54, 55]. This problem was studied by Ranz [56], who showed that the coupling of lamella deformation with diffusion can be reduced to a 1D diffusion reaction-diffusion equation by making use of (i) the rescaled coordinate perpendicular to the direction of lamella elongation and (ii) the so-called warped time that rescales temporal increments with the lamella elongation to eliminate the stretching term. Qualitative insights about the coupling of stretching-enhanced mixing and chemical reactions were obtained in [20, 57, 58] based on numerical simulations. Le Borgne et al. [25] investigated the impact of non-uniform flow conditions on the mixing and reaction rates under such conditions using a lamellar mixing front approach. Paster et al. [59] investigated the impact of shear upon reaction for uniformly initial distribution of reactants with concentration fluctuations.

Fluid stretching has been shown to play a fundamental role for governing mixing in porous media [60, 61, 62, 63, 64]. The presence of heterogeneity in the advective flow field invariably leads to lamella formation and subsequent coalescence [65, 66, 67, 68]. Therefore, understanding the interaction between the invading fluid and the residing fluid is imperative towards prediction of species transport in such media. For example, Mays and Neupauer [69] have demonstrated a methodology to achieve enhanced mixing inducing chaotic Darcy-like flow patterns. Gramling et al. [70] performed an experimental and theoretical Darcy scale study of the reaction rate and moving front width in a porous medium for the irreversible bimolecular reaction $A+B \rightarrow C$. They provided hints that incomplete pore-scale mixing was limiting local reaction rates, based on the inability of a Darcy scale modeling approach to properly predict the longitudinal concentration profiles and total mass of product. Later, de Anna et al. [24] investigated the impact of pore-scale mixing on chemical reactions in a two-dimensional (2D) porous medium consisting of cylindrical grains allowing to measure the 2D concentration field at the pore scale. They confirmed the role of mixing in controlling local reaction rates and were able to quantitatively predict the temporal evolution of the measured product mass

in the infinite Damköhler limit (i.e for fast reactions) using an upscaling theory based on the concept of lamellar reaction front [71]. Oates [72] and later Chiogna and Bellin [73] used a concentration probability density function (PDF) based mixing model to quantify the observed reaction rates in the experimental setup of Gramling et al. [70].

In this work, we focus on reactive mixing of the bimolecular reaction $A + B \rightarrow C$ under shear flow, which represents a fundamental fluid deformation and reaction process in porous media. Shear occurs for any situations where adjacent parallel streamlines have different velocities. At the pore scale, shear is created by strong velocity gradients near fluid-solid interfaces [24]. At the Darcy scale, shear flow is the dominant fluid stretching mechanism governing mixing and spreading in randomly stratified media, typical of sedimentary formations, where the horizontal correlation length is much larger than the vertical one [74, 75, 76, 77, 78]. More generally, shear plays an important role in heterogeneous porous media as one of the components of local deformation tensors [79, 66]. While linear shear flows give rise to a linear elongation of mixing fronts, other stretching dynamics could be considered in the same framework, such as power law [66] or exponential [80] deformation (which implies that the length of a material line increases in time following a power-law behaviour in time or increases exponentially). Hence, beyond the particular choice of shear flows, the general methodology presented here for predicting the effective reaction kinetics of mixing fronts from the coupling between the stretching dynamics and the characteristic reaction time scales is likely relevant for more complex flows. While the impact of fluid stretching on reaction kinetics is well understood for fast reactions [81, 25], the broad range of scales and the diversity of chemical reactions entails the need for accounting for a wide range of reaction time scales compared to the transport time scales, that is, for a wide range of Damköhler numbers [82, 83, 84]. Therefore, we investigate analytically and numerically the global reaction kinetics of a mixing front with two initially separated diffusive reactants subjected to velocity gradients of different magnitudes, for an arbitrary finite Damköhler number. In particular we are interested (i) in the rate at which the product is formed and (ii) in the temporal evolution of the width of the reaction front. From the analysis of asymptotic behaviors of pertinent equations we establish the existence of three distinct regimes of effective upscaled reaction kinetics that result from the interplay between reaction, diffusion and stretching. We pinpoint the transition times which demarcate the various regimes. We validate the analytical predictions derived for the temporal scalings of the product mass and the reaction mixing scale, i.e. the width of the reaction front, by comparison with numerical simulations.

2. Theoretical framework

2.1. System description and governing equations

We consider the scenario of two reactants A and B that are initially separated by an interface. The system is subjected to a linear shear flow perpendicular to the initial interface characterized by a constant

velocity gradient as shown in figure 1.a. The designated mass of reaction product grows and spreads owing to (a) diffusion, (b) advection (imposed shear flow) and (c) reaction at the interface between the two reactants. The rate of reaction is assumed to follow a second order kinetics given by $A + B \xrightarrow{k} C$ with k denoting the rate constant of the chemical reaction. We consider the following two coordinate systems illustrated in figure 1.b. The coordinate system (x, y) is fixed while the frame (x', y') is attached to the stretching interface so that the coordinate x' always corresponds to the direction perpendicular to the interface. The shear flow in the laboratory frame is denoted by $\tilde{\mathbf{u}} = (G\tilde{y}, 0)$. Owing to the action of the shear, the front stretches about the origin as the pivot. As stretching occurs along the interfacial direction, the thickness in the direction normal to the front decreases due to the constraint of continuity (that is, the fluid mass conservation). In other words, stretching of the fluid along the interface is accompanied by a compression in the perpendicular direction of the interface.

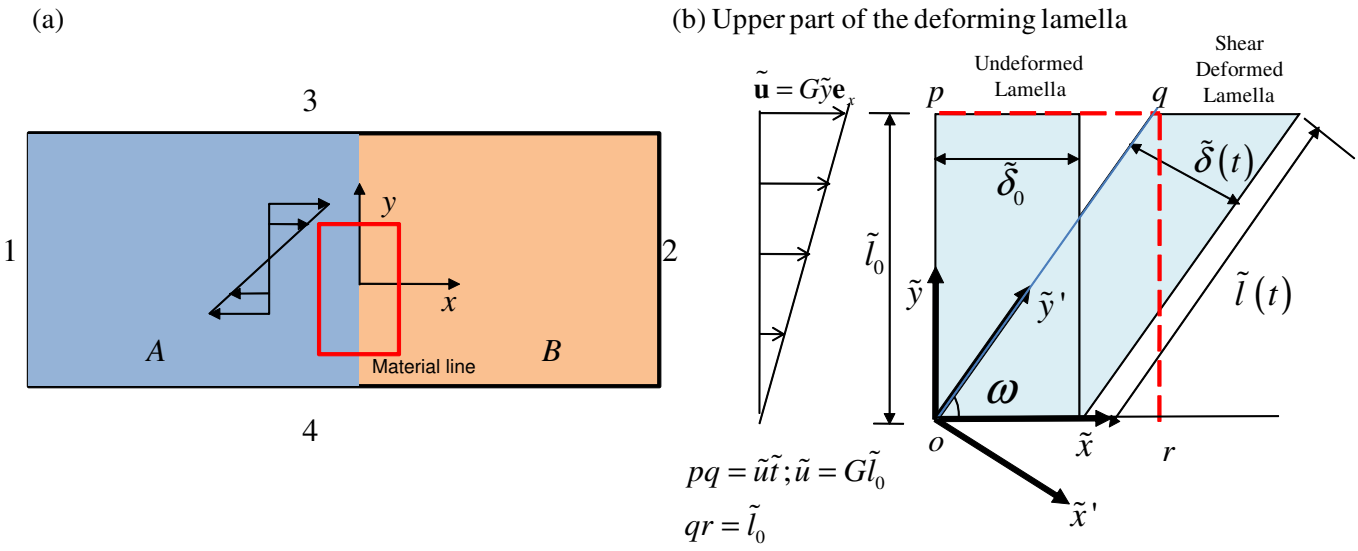

Figure 1: General schematic and description of the system employed for a 2D simulation of reaction-diffusion in the presence of a linear shear flow. (a) Boundaries 1 and 2 are considered to be periodic. Boundaries 3 and 4 are assigned to be no-flux for the 2D simulation. (b) We depict the upper part of the deforming lamella owing to the action of the shear flow pivoted around the point o, for a material line of initial width δ_0 and length $\tilde{l}$, deforming in the flow field so that its length increases to $\tilde{l}(t)$ and width reduces to $\delta(t)$. In the figure, the origin is fixed, the distance moved by the point p is the local velocity times the time. Considering a material line positioned at the center of the mixing zone in (a), we link the transport equations defined in the 2D system presented in (a) to a 1D transport process defined in the reference frame normal to the direction of deformation of the material line. The evolution of the system is then described as a function of a 1D coordinate x' which is normal to the stretching interface. The instantaneous angle with which the coordinate system has locally rotated can be found out through the arctan of the ratio of the lengths qr and or which are mentioned in the figure.

The transport of the reactant and product concentrations, $\tilde{a}$, $\tilde{b}$ and $\tilde{c}$ respectively (the symbols with tilde

represent dimensional quantities) is described by the following set of advection-reaction-diffusion equations

$$\begin{aligned}
\frac{\partial \tilde{a}}{\partial \tilde{t}} + \tilde{\mathbf{u}} \cdot \nabla \tilde{a} &= D\nabla^2 \tilde{a} - k\,\tilde{a}\tilde{b}, \\
\frac{\partial \tilde{b}}{\partial \tilde{t}} + \tilde{\mathbf{u}} \cdot \nabla \tilde{b} &= D\nabla^2 \tilde{b} - k\,\tilde{a}\tilde{b}, \\
\frac{\partial \tilde{c}}{\partial \tilde{t}} + \tilde{\mathbf{u}} \cdot \nabla \tilde{c} &= D\nabla^2 \tilde{c} + k\,\tilde{a}\tilde{b},
\end{aligned} \tag{1}$$

where D is a constant and represents the diffusion coefficient of the species.

Equation (1) is subjected to the following initial conditions:

$$\begin{aligned}
\tilde{a}\,(\tilde{\mathbf{x}}, 0) &= \begin{cases} \tilde{n}_0 & \text{if } \tilde{x} < 0, \forall \tilde{y} \\ 0 & \text{otherwise} \end{cases}, \\
\tilde{b}\,(\tilde{\mathbf{x}}, 0) &= \begin{cases} 0 & \text{if } \tilde{x} \geq 0, \forall \tilde{y} \\ \tilde{n}_0 & \text{otherwise} \end{cases}, \\
\tilde{c}\,(\tilde{\mathbf{x}}, 0) &= 0 \ \forall \tilde{\mathbf{x}} \ .
\end{aligned} \tag{2}$$

The velocity field is given by $\tilde{\mathbf{u}} = G\tilde{y}\mathbf{e}_x$ with G representing the shear rate. The boundary conditions for the species A and B are that the top and bottom (walls 3 and 4) are no flux walls while the left and right walls (walls 1 and 2) are periodic (the effect of this periodicity is observed in the concentration distribution depicted in figure B.12 and figure B.12). These conditions are written down for solving for the species transport in a finite domain keeping in mind that we want to mimick a front where ideally the two domains are infinitely long. In such a system over a sufficient amount of time, there is no influence of time up until which the periodic image of the concentration interacts with itself. Beyond this time, the predictions of the 2D simulations would no longer be valid for an isolated front but would represent the situation where there is overlapping of concentration profiles (boundary effects; this would imply longer times than those shown in figure B.12). There is, thus, no specific length scale attached to the problem; this is akin to most semi-infinite problems for diffusion, such as observed in heat transfer and mass transfer in a semi-infinite domain [85, 86]). Hence, to address the problem computationally for the 2D simulations, we have enforced periodic boundary conditions at the left and right boundaries in such a way that over the time of observation, the system does not experience the effects of the boundaries.

We nondimensionalize equation (1) by the following quantities:

$$\mathbf{x} = \tilde{\mathbf{x}}/\tilde{\delta_0}\ , t = \tilde{t}D/\tilde{\delta_0^2},\ \mathbf{u} = \tilde{\mathbf{u}}/G\tilde{\delta_0}\ , \phi = \tilde{\phi}/\tilde{n}_0\ ,\ \phi = a, b, c, \tag{3}$$

where in the system under consideration we choose the characteristic length to be of δ_0, the characteristic time scale of the system based on the characteristic length, $\tilde{\delta_0^2}/D$, the characteristic velocity of the system is proportional to the rate of shear times the characteristic length. Proceeding based on this nondimension-

alization, and defining the Péclet and Damköhler numbers as,

$$\begin{aligned} \mathsf{Pe} &= \frac{\tau_D}{\tau_a} = \frac{G\tilde{\delta}_0^2}{D}, \\ \mathsf{Da} &= \frac{\tau_D}{\tau_r} = \frac{k\tilde{n_0}\tilde{\delta_0}^2}{D}, \end{aligned} \tag{4}$$

which represent respectively the ratio of the typical diffusion time scale $\tau_D = \tilde{\delta}_0^2/D$ to the typical advection time scale $\tau_a = G^{-1}$ and that of the typical diffusion time scale to the typical reaction time scale respectively $\tau_r = (k\tilde{n_0})^{-1}$, equations (1) and (2) may be then recast as:

$$\begin{aligned} \frac{\partial a}{\partial t} + \mathsf{Pe}\,\mathbf{u}\cdot\nabla a &= \boldsymbol{\nabla}^2 a - \mathsf{Da}\,a\,b, \\ \frac{\partial b}{\partial t} + \mathsf{Pe}\,\mathbf{u}\cdot\nabla b &= \boldsymbol{\nabla}^2 b - \mathsf{Da}\,a\,b, \\ \frac{\partial c}{\partial t} + \mathsf{Pe}\,\mathbf{u}\cdot\nabla c &= \boldsymbol{\nabla}^2 c + \mathsf{Da}\,a\,b, \end{aligned} \tag{5}$$

subjected to the initial conditions

$$\begin{aligned} a(\mathbf{x},0) &= \begin{cases} 1 \text{ if } x < 0, \forall y \\ 0 \text{ otherwise} \end{cases}, \\ b(\mathbf{x},0) &= \begin{cases} 0 \text{ if } x \geq 0, \forall y \\ 1 \text{ otherwise} \end{cases}, \\ c(\mathbf{x},0) &= 0 \quad \forall \mathbf{x}\ . \end{aligned} \tag{6}$$

As we shall see later, depending on the relative strengths of Pe and Da the system evolution exhibits markedly different dynamics.

Note that the scenario where there is no definite length scale associated with the particular problem under consideration can be tackled in the following manner. A system lacking a characteristic lengthscale is akin to analysis pertaining to semi-infinite domains where the pertinent lengthscale must be obtained by a combination of the physically relevant parameters in the system [87]. In the context of the present problem, we may define two length scales based on the combination of the diffusion coefficient, D, the reaction kinetics constant, k, and the average shear rate, G. If the system is thought to evolve based on the balance of diffusion and reaction kinetics the length scale $\tilde{\delta}_0$ may be recast as $\sqrt{D/(kn_0)}$, which is obtained by comparing the characteristic lengthscale of molecular diffusion during the time τ_r, i.e. $\sqrt{D\tau_r}$, over the the characteristic reaction time $\tau_r = 1/(kn_0)$. On the other hand, if the system evolves based on the balance of diffusion and stretching, the lengthscale $\tilde{\delta}_0$ may be recast as $\sqrt{D/G}$, which is obtained by comparing the characteristic diffusion lengthscale to the stretching time $\tau_s = 1/G$. In the present derivation, we do not restrict ourselves to the choice of $\tilde{\delta}_0$ thereby allowing us to generalize the analysis presented here.

2.2. Reaction-diffusion system in a Lagrangian frame

To derive analytical expressions quantifying the coupling between reaction, diffusion and shear , we simplify the equations and make them more tractable by reducing the dimensionality of the problem [56, 88, 89, 54]. In order to provide a better insight into the fundamental process of stretching augmented reactive mixing, we convert the 2D transport problem defined in the laboratory frame to a one-dimensional (1D) transport problem defined in the local Lagrangian frame attached to a particular material point and rotating with the flow. A material line is a purely kinematic quantity, independent of the species residing in it [56], but we choose the material line that coincides with the middle line of the mixing zone (see Figure 1), which is initially oriented along the direction y. Considering a volume of initial constant thickness $\tilde{\delta}_0$ around the material line (also referred to as a lamella, see figure 1), the elongation of the line by shear deformation $\tilde{\rho}(t)$ leads to a simultaneous compression of the thickness $\tilde{\delta}$ (owing to incompressibility), such as [56, 90]. We therefore confine our attention to the region at the interface of the two reactants and track it as it evolves with the flow.

The advection-diffusion-reaction equation (1) for species $\tilde{a}$ may be simplified by expressing it in the coordinate system $(\tilde{x}', \tilde{y}')$ attached to a material line (Figure 1) [e.g., 56] . The simultaneous effect of compression, diffusion and reaction is quantified in a Lagrangian frame as follows (see Appendix A for the detailed derivation):

$$\frac{\partial \tilde{a}}{\partial \tilde{t}} - \Omega \tilde{x}' \frac{\partial \tilde{a}}{\partial \tilde{x}'} = D \frac{\partial^2 \tilde{a}}{\partial \tilde{x}'^2} - k\tilde{a}\tilde{b}, \tag{7}$$

and correspondingly for species $\tilde{b}$ and $\tilde{c}$. We have defined here the stretching rate

$$\Omega = -\frac{1}{\tilde{\delta}} \frac{d\tilde{\delta}}{d\tilde{t}}, \tag{8}$$

where $\tilde{\delta}$ is the width of a material strip whose initial orientation is perpendicular to the flow direction and whose initial length is $\tilde{\delta}_0$ (see Appendix A),

$$\tilde{\delta} = \frac{\tilde{\delta}_0}{\sqrt{1 + G^2 \tilde{t}^2}} \ . \tag{9}$$

It is observed in equation (7) that species evolution is only in the direction transverse to the elongation, that is $\tilde{x}'$. This stems from the fact that for a linear shear, concentration gradients are zero in the direction of elongation and exist only in the direction of compression [19, 56]. Even for arbitrary flows equation (7) is still a good approximation since concentration gradients are continuously maximized in the direction of compression [54, 66] (Please refer to Appendix A for a discussion).

We can make further progress by transforming the above equation into a diffusion-reaction system by making use of the following rescaled variables [56]:

$$z = \frac{\tilde{x}'}{\tilde{\delta}} \quad \text{and} \quad \theta = \int_0^{\tilde{t}} d\tau \ \frac{D}{\tilde{\delta}(\tau)^2} \ . \tag{10}$$

where θ is referred to as the warped time which represents the integral diffusion time over the lamella thickness. The transformed spatial coordinate, z, must not be confused with the z coordinate in the usual orthogonal three-dimensional Cartesian system. We obtain:

$$\begin{aligned}
\frac{\partial \tilde{a}}{\partial \theta} &= \frac{\partial^2 \tilde{a}}{\partial z^2} - k\tilde{a}\tilde{b}\frac{\tilde{\delta}^2}{D}, \\
\frac{\partial \tilde{b}}{\partial \theta} &= \frac{\partial^2 \tilde{b}}{\partial z^2} - k\tilde{a}\tilde{b}\frac{\tilde{\delta}^2}{D}, \\
\frac{\partial \tilde{c}}{\partial \theta} &= \frac{\partial^2 \tilde{c}}{\partial z^2} + k\tilde{a}\tilde{b}\frac{\tilde{\delta}^2}{D}.
\end{aligned} \tag{11}$$

Furthermore, a nondimensionalization may be employed for the lamella thickness as $\delta = \tilde{\delta}/\tilde{\delta}_0$, and by taking advantage of equation (8) we may simplify the definition of the warped time to obtain the form

$$\theta = \int_0^{\tilde{t}} \frac{d\tau}{\tilde{\delta}\left(\tau\right)^2/D} = \frac{D}{\tilde{\delta}_0^2}\int_0^{\tilde{t}} d\tau \left(1 + G^2\tilde{\tau}^2\right) = \frac{D}{\tilde{\delta}_0^2}\left(\tilde{t} + \frac{G^2\tilde{t}^3}{3}\right) \quad . \tag{12}$$

where we have used the fact that at $\tilde{t} = 0$, $\theta = 0$. Using this, and the aforementioned nondimensional scheme, we may write the governing equations in the Lagrangian frame for the three species in the frame attached with the deforming material line as

$$\begin{aligned}
\frac{\partial a}{\partial \theta} &= \frac{\partial^2 a}{\partial z^2} - \mathsf{Da}\, ab\delta^2, \\
\frac{\partial b}{\partial \theta} &= \frac{\partial^2 b}{\partial z^2} - \mathsf{Da}\, ab\delta^2, \\
\frac{\partial c}{\partial \theta} &= \frac{\partial^2 c}{\partial z^2} + \mathsf{Da}\, ab\delta^2,
\end{aligned} \tag{13}$$

where the Péclet number and Damköhler numbers have already been defined in section 2.1 and

$$\delta = \frac{1}{\sqrt{1 + \mathsf{Pe}^2 t^2}} \tag{14}$$

from equation (9)).

The solution for the set of equations (11) yields the temporal and spatial evolution for the concentration fields of the different species. The initial conditions specified for solving equation (11) are that as $z \to -\infty$, $a = 1, b = 0$ and that as $z \to \infty$, $b = 1, a = 0$. The aim of the present work is to depict how the chemical kinetics constants in conjunction with the lamella stretching impact the mass of the product formed in such a scenario.

We may write the mass of the product as $\tilde{m}_c = \int_{-\infty}^{\infty} d\tilde{x}'\tilde{c}(x')l(t)$, where $l(t)$ represents the length of the interface. In a nondimensional sense, it may be recast as

$$m_c = \frac{\tilde{m}_c}{n_0 l_0 \tilde{\delta}_0} = \int_{-\infty}^{\infty} dz\, c(z) l\delta = \int_{-\infty}^{\infty} dz\, c(z) \ , \tag{15}$$

where we have made use of the fact that $l\delta = 1$ (owing to the incompressibility condition which imposes that the amount of longitudinal stretching be the inverse of the amount of transverse compression in order to conserve the material volume).

Another quantity of interest is the reactive mixing scale, which quantifies the spatial localization of chemical reactivity in a mixing front [27]. A small reactive mixing scale denotes the existence of localized hotspots of chemical reaction, while a large reactive mixing scale implies that the reaction zone is diffuse. The reactive mixing scale is thus an important characteristic of reactive fronts, which, as discussed in the following, depends non-trivially on Pe, Da and on the observation time. The reactive mixing scale can be estimated from the width of the reaction front from the second moment of the reaction rate across the front as

$$\tilde{s}_r = \left(\frac{\int_{-\infty}^{\infty} d\tilde{x}' \, \tilde{x}'^2 \mathsf{Da} ab}{\int_{-\infty}^{\infty} d\tilde{x}' \, \mathsf{Da} ab} \right)^{1/2} , \tag{16}$$

In a nondimensional sense, it can be written in terms of the integral in the transformed coordinate, z, as

$$s_r = \left(\frac{\int_{-\infty}^{\infty} dz \, z^2 \mathsf{Da} \, ab}{\int_{-\infty}^{\infty} dz \, \mathsf{Da} \, ab} \right)^{1/2} \delta \, . \tag{17}$$

Note that the reactive mixing scale is different from the conservative mixing scale [91, 66] since it is affected by chemical reactions that tend to reduce it through consumption of reactants. Besides the temporal evolution of the mass of the product, the temporal evolution of the width of the reaction zone is also of interest and is analyzed in section 4. The initial reaction width, i.e. $s_r(0)$, will be referred to as s_0.

3. Analytical predictions for the temporal evolution of the mass of product

Having discussed the general 1D framework used to investigate the transport of reactive species, we focus on the various limits of the temporal evolution of the mass of product. Let us remind here that the Péclet number denotes the ratio of the typical diffusion time scale (over the distance δ_0) to the typical advection time scale (due to the fluid shear), while the Damköhler number denotes the ratio of the typical reaction time scale to the typical diffusion time scale. This implies that the dimensionless time $t = \tilde{t}/\tau_D$ allows us to distinguish the dynamics of the systems in terms of the relative values of $\mathsf{Pe}^{-1} = \tau_a/\tau_D$ and $\mathsf{Da}^{-1} = \tau_r/\tau_D$.

The first scenario, termed as *weak stretching* scenario, is defined by a system for which $Da^{-1} < Pe^{-1}$. In such a scenario, 3 different time regimes can be distinguished. The first regime occurs for a dimensionless time $t \ll Da^{-1}$. Here the reaction dynamics is determined by the interaction of diffusion and reaction kinetics since the time is small compared to the characteristic reaction time. In the second regime, occurring for $\mathsf{Da}^{-1} < t < \mathsf{Pe}^{-1}$, the reaction is diffusion limited since the time is large compared to the reaction time (i.e. reactions are fast) but small compared to the characteristic shear time (i.e. stretching does not play a role yet). In the asymptotic long time regime, $t \gg \mathsf{Pe}^{-1}$, the shear action of the flow field is activated and the reaction kinetics is controlled by stretching-enhanced diffusion.

The second scenario, termed as the *strong stretching* scenario is defined as $\mathsf{Pe}^{-1} < \mathsf{Da}^{-1}$. The first regime, characterized by a dimensionless time $t \ll \mathsf{Pe}^{-1}$ is similar to the first regime in the weak stretching

case. The system is dominated by the interaction of diffusion and reaction kinetics. The second time regime, for which $\mathsf{Pe}^{-1} < \mathsf{Da}^{-1}$, sees a reaction behavior that results from the interaction of the reaction kinetics and stretching enhanced diffusion as time is large enough for stretching to be activated but small compared to the characteristic reaction time. This regime is particularly interesting as stretching and reaction kinetics are fully coupled. In the long time regime, $t \gg \mathsf{Da}^{-1}$, the reaction behavior is fully limited by stretching-enhanced diffusion as reaction kinetics is no longer limiting.

As detailed in the introduction, reaction front kinetics have been investigated mostly in the limits $t \ll \mathsf{Pe}^{-1}$ (no shear) or $t \gg \mathsf{Da}^{-1}$ (fast reactions under shear), which represents only a subset of the range of possible regimes described above. In the following we derive the temporal evolution of the product mass for all the aforementioned regimes.

3.1. Weak stretching scenario: $Da^{-1} < Pe^{-1}$

For a dimensionless time $t \ll \mathsf{Pe}^{-1}$ shear does not affect the reactive transport behavior as both the elongation ρ and the width δ are approximately constant (see equation (9)). Thus, the evolution of the product c can be represented by the diffusion reaction equation

$$\frac{\partial c}{\partial t} = \frac{\partial^2 c}{\partial x^2} + \mathsf{Da} ab. \tag{18}$$

Hence, this regime is akin to the case where there is no imposed flow field [27]. Conversely for $t \gg \mathsf{Pe}^{-1}$, shear plays an important role in increasing the area available for diffusive mass transfer, and enhancing chemical gradients by compression. In the following, we discuss the three regimes separated by the characteristic times Da^{-1} and Pe^{-1}.

3.1.1. Reaction-diffusion regime (negligible shear): $t \ll Da^{-1}$

In this regime, the initial profiles of a and b both evolve due to diffusion while the impact of reaction is still weak. In such a case, the concentration profiles of the two reactants can be approximated by the diffusive profiles [85]

$$a = \frac{1}{2}(1 + \mathrm{erf}(x/2\sqrt{t})), \tag{19}$$

$$b = \frac{1}{2}(1 - \mathrm{erf}(x/2\sqrt{t})), \tag{20}$$

Thus, in this regime where we can neglect the effect of shear, we may write the evolution of c, inserting equation (19) and (20) in equation (18), as

$$\frac{\partial c}{\partial t} = \frac{\partial^2 c}{\partial x^2} + \mathsf{Da}\frac{1}{4}\left[1 - \mathrm{erf}\left(\frac{x}{2\sqrt{t}}\right)^2\right] \tag{21}$$

which, in the vicinity of the interface, i.e. the origin (where most of the product is formed) may be further simplified as

$$\frac{\partial c}{\partial t} = \frac{\partial^2 c}{\partial x^2} + \mathsf{Da}\frac{1}{4}. \tag{22}$$

We may integrate this over space to obtain the temporal evolution of the mass of product formed as

$$\frac{\partial m_c}{\partial t} = \left[\frac{\partial c}{\partial x}\right]_{-\infty}^{\infty} + \frac{\mathsf{Da}}{4} s_r \tag{23}$$

wherein the second term on the right hand side has a contribution from $\mathsf{Da}/4$ which is concentrated near the interface (at the origin), while s_r represents the reactive mixing scale. The first term on the right hand size is zero on account of the fact that the concentration profile decays away from the front towards either reactant so that $\partial c/\partial x(x \to \pm\infty) = 0$. Now, at such times where $t \ll \mathsf{Pe}^{-1}$ and $t \ll \mathsf{Da}^{-1}$, the growth of the reactive mixing scale is only *diffusion controlled*, which leads to the growth of the reactive mixing scale as $s_r \sim \sqrt{t}$. Thus, we arrive at the evolution of m_c by integrating equation (23) in time as

$$m_c \approx \frac{\mathsf{Da}}{4} t^{3/2}. \tag{24}$$

This result is equivalent to that obtained by Arshadi and Rajaram [29] in the early time regime of a reaction front with no shear.

3.1.2. Diffusion limited regime (negligible shear at intermediate times): $\mathsf{Da}^{-1} < t < \mathsf{Pe}^{-1}$

In order to determine the behavior at longer times (where the reactions are fast and the influence of the shear is still not present; this regime is similar to the case at long times in the absence of any imposed flow), we follow the lead of Larralde et al. [27]. For completeness, we summarize here the main steps of the derivation and the key results. We begin by representing the concentration of the product as a perturbation on the diffusive case. Formally, we first observe that the concentrations of the two reactants may be written as $a = F + g$ and $b = g$ where $F = a - b$ satisfies the conservative equation (by noting that subtracting the two concentration fields eliminates the nonlinearity of the reaction term)

$$\frac{\partial F}{\partial t} = \frac{\partial^2 F}{\partial x^2} \quad . \tag{25}$$

where g represents the concentration perturbation. Consequently, the governing equation for g may be represented as

$$\frac{\partial g}{\partial t} = \frac{\partial^2 g}{\partial x^2} - \mathsf{Da}\, g \left(\mathrm{erf}\left(\frac{x}{\sqrt{4t}}\right) + g\right) \tag{26}$$

which may be simplified by neglecting the nonlinear contribution from g^2 (since g is considered to be a perturbation to F) and linearizing $\mathrm{erf}(x/\sqrt{4t})$ for times so large and the point of interest such that $x/\sqrt{4t} \ll 1$, we obtain

$$\frac{\partial g}{\partial t} \approx \frac{\partial^2 g}{\partial x^2} - \mathsf{Da}\, g \frac{x}{\sqrt{\pi t}} \quad . \tag{27}$$

At times sufficiently long for the temporal derivative to be negligible, the time behaves as a parameter to the Airy differential equation given by: $\frac{\partial^2 g}{\partial x^2} - \mathsf{Da}\, g \frac{x}{\sqrt{\pi t}} = 0$. The solution to this may be written by resorting to an Airy function, as [27]:

$$g \sim f(t)\, Ai\left(\lambda \frac{x}{t^{1/6}}\right),\ \lambda = \left(\frac{\mathsf{Da}}{\sqrt{\pi}}\right)^{1/3} \quad . \tag{28}$$

We may assume a power-law representation for the function $f(t)$ so that the form for the concentration perturbation is represented as $g = \psi t^{\alpha} Ai(\lambda x/t^{1/6})$. By equating the form of the nonlinear term in (26) and the spatial derivative term on the right hand side of equation (28), we see that $\alpha = -1/3$ and $\psi = 1/\lambda$. Thus, the perturbation to the concentration is found out as

$$g \sim \frac{t^{-1/3}}{\lambda} Ai\left(\frac{\lambda x}{t^{1/6}}\right) \quad . \tag{29}$$

The above may be further simplified for the case of large enough x such that $\lambda x \gg t^{1/6}$ to yield

$$g \sim \frac{t^{-1/3}}{\lambda}\left(\frac{\lambda x}{t^{1/6}}\right)^{-1/4} \exp\left(-\frac{2}{3}\left(\frac{\lambda x}{t^{1/6}}\right)^{3/2}\right) \quad , \tag{30}$$

while the reaction term may be recast based on Eq.(27)) to yield

$$R \sim \mathsf{Da}\frac{x}{\sqrt{t}}\frac{t^{-1/3}}{\lambda}\left(\frac{\lambda x}{t^{1/6}}\right)^{-1/4} \exp\left(-\frac{2}{3}\left(\frac{\lambda x}{t^{1/6}}\right)^{3/2}\right) \quad . \tag{31}$$

The time integral of the reaction term may then be obtained as $I \sim \int_0^{\infty} R dt$, which, according to equation (31) can be written as

$$I \sim \int_0^{\infty} dt \mathsf{Da}\frac{x}{\sqrt{t}}\frac{t^{-1/3}}{\lambda}\left(\frac{\lambda x}{t^{1/6}}\right)^{-1/4} \exp\left(-\frac{2}{3}\left(\frac{\lambda x}{t^{1/6}}\right)^{3/2}\right) \quad . \tag{32}$$

Upon simplification, equation (32) can be written, in leading order, as

$$I \sim \lambda t^{1/3}\left(\frac{\lambda x}{t^{1/6}}\right)^{-3/4} \exp\left(-\frac{2}{3}\left(\frac{\lambda x}{t^{1/6}}\right)^{3/2}\right) \tag{33}$$

Towards determining the mass of product, we appeal to the above equation and equation (15) to obtain

$$m_c = 2\int_0^{\infty} dx \lambda t^{1/3}\left(\frac{\lambda x}{t^{1/6}}\right)^{-3/4} \exp\left(-\frac{2}{3}\left(\frac{\lambda x}{t^{1/6}}\right)^{3/2}\right)$$

where the factor of 2 appears when the spatial integration is done from the lower bound 0 instead of $-\infty$ while keeping in mind that the integral is symmetric for the concentration perturbation. The integral can be evaluated by making the change of variable $\beta = \lambda x/t^{1/6}$ to obtain

$$m_c \approx t^{1/2} 2\int_0^{\infty} d\beta \exp\left(\frac{2}{3}\beta^{3/2}\right)\beta^{-3/4} \approx 8t^{1/2} \quad . \tag{34}$$

The general observation is that the temporal evolution of the mass of the product formed in this regime becomes independent of the Damköhler number, which is expected for this regime that is purely diffusion-limited. We note here that the integral appearing in equation (34) comes out to be $2\int_0^{\infty} dx \exp(2x^{3/2}/3)x^{-3/4} = 2/3 \times (2^{5/6}3^{1/6}\pi/)\Gamma(5/6)$ whose approximate value is 7.94, and which we further approximate as 8 in the equation above. This result is in line with the derivation of Larralde [27] and of Arshadi and Rajaram [29] for a reactive front with no shear.

3.1.3. Shear-enhanced reactive mixing regime: $t \gg \mathsf{Pe}^{-1}$

We now turn our attention to the case where the imposed velocity gradient has significant bearing on the dynamics of the reaction-diffusion system. Towards analyzing this, we begin with equation (11) and move ahead with the logic similar to that employed in section 3.1.2. In $z-\theta$ coordinates, which account for the effect of shear-induced elongation and compression of the interface, we may write the evolution of the perturbation to the concentrations of a and b, as in equation (26), as

$$\frac{\partial g}{\partial \theta} = \frac{\partial^2 g}{\partial z^2} - \frac{\mathsf{Da}}{1+\mathsf{Pe}^2 t^2} g \left(\mathrm{erf}\left(\frac{z}{\sqrt{4\theta}} \right) + g \right) \ , \tag{35}$$

which can be further simplified by neglecting the nonlinear contribution of the g^2 term to yield

$$\frac{\partial g}{\partial \theta} = \frac{\partial^2 g}{\partial z^2} - \frac{\mathsf{Da}}{1+\mathsf{Pe}^2 t^2} g \frac{z}{\sqrt{\pi\theta}} \ . \tag{36}$$

For $t > \mathsf{Pe}^{-1}$, we can approximate $1/1+\mathsf{Pe}^2 t^2 \approx 1/\mathsf{Pe}^2 t^2$. We consider the system in the x' and t coordinates which are easily transformed by recalling that $z = x'/\delta \sim x' \mathsf{Pe}\, t$ and $\theta \sim \mathsf{Pe}^2 t^3/3$, obtaining

$$\frac{\partial g}{\partial t} = \frac{\partial^2 g}{\partial x'^2} - \mathsf{Da}\sqrt{\frac{3}{\pi}} g \frac{x'}{t} \ . \tag{37}$$

The solution to equation (37) may be obtained (in analogous manner to that in section 3.1.2) as

$$g \approx \frac{t^{-1/3}}{\lambda'} Ai\left(\frac{\lambda' x'}{t^{1/6}} \right) \ , \tag{38}$$

where $\lambda' = (\mathsf{Da}\sqrt{3/\pi})^{1/3}$. Proceeding, we may write the rate of reaction term as

$$R = \mathsf{Da} \frac{x'}{t^{1/2}} g \approx \lambda'^3 \frac{x'}{t^{1/2}} \times \frac{t^{-1/3}}{\lambda'} Ai\left(\frac{\lambda' x'}{t^{1/6}} \right) \ , \tag{39}$$

which we may simplify to obtain

$$R \approx \lambda' \left(\frac{\lambda' x'}{t^{1/6}} \right) t^{-2/3} Ai\left(\frac{\lambda' x'}{t^{1/6}} \right) \ . \tag{40}$$

Proceeding further, we may integrate the above expression in space and time to obtain

$$m_c \approx \lambda' t^{1/3} 2 \int_0^\infty dz \left(\frac{\lambda' x'}{t^{1/6}} \right)^{-3/4} \exp\left(-\frac{2}{3} \left(\frac{\lambda' x'}{t^{1/6}} \right)^{3/2} \right) \ , \tag{41}$$

the evaluation of the integral over the z space necessitates converting the groups of the variables into the form of $\gamma = (\lambda z)/(\mathsf{Pe}\, t^{7/6})$ (the conversion of the variable from x' in terms of z results in the appearance of Pe through the relation $z \sim x' \mathsf{Pe} t$ as noted earlier). Performing this, we obtain from equation (41) that

$$m_c \approx 8 \mathsf{Pe}\, t^{3/2} \ . \tag{42}$$

This expression shows that, as expected, the impact of the shear action of the flow leads to a stronger increase in the product mass than that due to pure diffusion as given by equation (34). This result is validated against numerical simulations in section 6.

It is interesting to note however that the scaling is the same as in the kinetics limited regime (equation 25). For the weak stretching scenario, discussed in this section, the effects of kinetics limitation, due to finite reaction times, are confined to the domain of dimensionless times $t \ll \mathsf{Da}^{-1}$, while the effects of mixing enhancement by shear are confined to the domain $t \gg \mathsf{Pe}^{-1}$. Hence, as $\mathsf{Da}^{-1} < \mathsf{Pe}^{-1}$, these two domains are disjoint and these two effects are decoupled. As discussed in the next section, this is not the case for the strong stretching scenario, which leads to new scaling laws.

3.2. Strong stretching scenario: $Pe^{-1} < Da^{-1}$

In the strong stretching scenario, the shear time scale Pe^{-1} is smaller than the characteristic reaction scale Da^{-1}. In this scenario, the diffusion-limited reaction regime $\mathsf{Da}^{-1} < t < \mathsf{Pe}^{-1}$ does not exist. Instead, we find a new regime characterized by the interaction of stretching-enhanced mixing and reaction. It must first be noted that for a dimensionless time $t \ll \mathsf{Pe}^{-1}$ the effect of stretching, as manifested through the presence of the term δ^2 in the reaction term (where we recall that $\delta = 1/\sqrt{1+\mathsf{Pe}^2 t^2}$), is weak, and thus the approximate equations assuming $1 + \mathsf{Pe}^2 t^2 \approx 1$ result in the analysis seen in section 3.1.1. Essentially this implies that in the initial time, the system behaves as if there is no imposed shear. On the other hand, in the long time regime ($t \gg \mathsf{Da}^{-1}$), the reaction behavior is the same as the one obtained in section 3.1.3, i.e. that of shear-enhanced reactive mixing with no kinetics . In the following, we therefore only study the reaction behavior in the intermediate regime ($\mathsf{Pe}^{-1} < t < \mathsf{Da}^{-1}$) in which the effect of flow stretching and kinetics limitations are both non-negligible. We thus begin the analysis through equation (13) in terms of $z - \theta$ coordinates:

$$\frac{\partial c}{\partial \theta} = \frac{\partial^2 c}{\partial z^2} + \mathsf{Da} ab\delta^2 \quad , \tag{43}$$

As in section 3.1.1, approximating the profiles of a and b by diffusive profiles, which are weakly affected by reaction, and linearizing close to $z = 0$, this expression can be integrated over z ans simplified to obtain (using the arguments that $\partial c/\partial z(z \to \pm\infty) = 0$)

$$\frac{\partial m_c}{\partial \theta} \approx \frac{\mathsf{Da}}{4}\delta^2 s_r \quad . \tag{44}$$

Note that this expression is based on the same approximations as equation (23) but it is here written in $\{\theta, z\}$ coordinates to account for shear. Recalling that $d\theta/dt = 1/\delta^2$, we can rewrite equation (44) as

$$\frac{\partial m_c}{\partial \theta} \approx \frac{\mathsf{Da}}{4}\left(\frac{d\theta}{dt}\right)^{-1} s_r \implies \frac{\partial m_c}{\partial t} \approx \frac{\mathsf{Da}}{4}\sqrt{\theta} \quad . \tag{45}$$

where we have made use of the fact that during this warped time, the diffusive growth of the width is proportional to $\sqrt{\theta}$. By utilizing the form of the warped time, $\theta = \left(t + \mathsf{Pe}^2 t^3/3\right) \sim \mathsf{Pe}^2 t^3/3$, we finally obtain

$$\frac{\partial m_c}{\partial t} \approx \frac{\mathsf{DaPe}}{4\sqrt{3}} t^{3/2} \implies m_c \approx \frac{\mathsf{DaPe}}{10\sqrt{3}} t^{5/2} \quad . \tag{46}$$

Hence, it is observed that the coupling of shear-enhanced mixing and kinetics limitations leads to a strong acceleration of the effective kinetics, which is faster than all previously known regimes. Consistently, the mass produced is proportional to both Da and Pe.

Figure 2 synthesizes the different regimes expected from the analysis for the scaling of the mass of produced in mixing fronts. The new coupled stretching and kinetics regime, that shows accelerated mass production $m_c \sim \mathsf{PeDa}t^{5/2}$, appears to cover a significant part of the diagram. The presented analytical derivations thus provide a unified theoretical framework covering the full space of Pe, Da and t parameters.

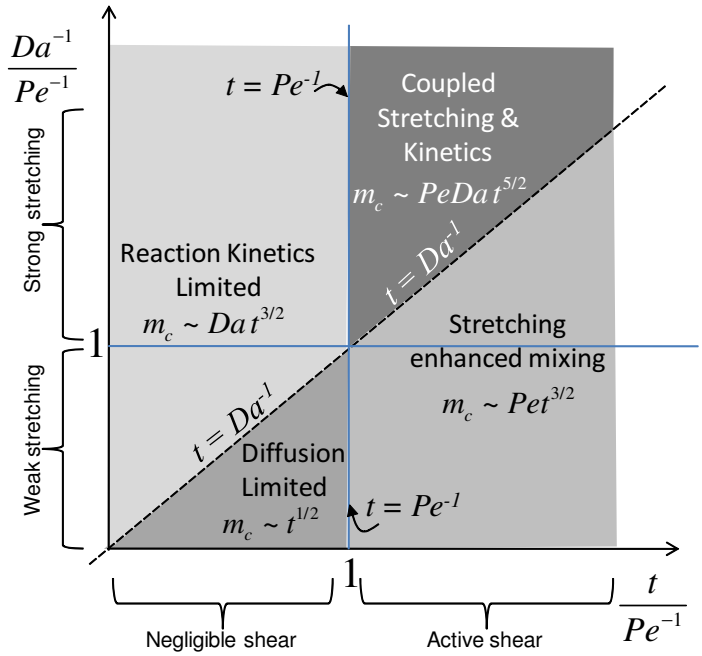

Figure 2: Diagram synthesizing the different regimes predicted for the scaling of the mass of product. The $y-$axis represents the two vertical separations of weak stretching and strong stretching when $\mathsf{Da}^{-1}/\mathsf{Pe}^{-1} < 1$ and > 1 respectively. The $x-$axis is also demarcated by the regimes of negligible shear and strong shear through $t/\mathsf{Pe}^{-1} < 1$ and > 1 respectively. We recall that t is the dimensionless time $t = \tilde{t}D/\tilde{\delta}_0^2$.

3.3. Transition times

In this section, we quantify more precisely the transition times between the different regimes discussed above. Quite naturally, in the absence of any imposed shear flow, we would expect the presence of only one dimensionless transition time at Da^{-1} between the kinetics-limited regime, discussed in section 3.1.1, and the diffusion-limited regime, discussed in section 3.1.2. The interest of the problem under consideration lies in configurations with significant imposed stretching. Depending on the relative strength of the stretching and reaction kinetics, we may have various transitions occurring as time progresses. We shall discuss these in details below.

Let us first consider the scenario of weak stretching $\mathsf{Da}^{-1} < \mathsf{Pe}^{-1}$. In this case, the system is expected to have two transitions. The first transition occurs between the early time kinetics-limited regime and the intermediate diffusion-limited regime, while the second transition occurs between the intermediate diffusion-limited reaction regime and the long time shear-enhanced reactive mixing regime. Towards determining the first transition time we must have an overlap of the product formed between these regions so that $\mathsf{Da}/4t^{3/2} = 8t^{1/2}$ (see sections 3.1.1 and 3.1.2)). This yields the dimensionless transition time as $t_{\mathsf{Da}_1} = 32/\mathsf{Da}$. Consequently, the mass of product at this transition may be found out as $m_{c,\mathsf{Da}_1} = 45/\sqrt{\mathsf{Da}}$. Moving on to the second transition from the diffusion-limited reaction regime (section 3.1.2) to the long time shear-mixing-limited reaction regime (section 3.1.3), we equate the masses of product for the two regimes, obtaining $8t^{1/2} = 8\mathsf{Pe}t^{3/2}$, which yields a characteristic dimensionless time $t_{\mathsf{Pe}_1} = \mathsf{Pe}^{-1}$. In this case the mass of product at the transition is given by $m_{c,\mathsf{Pe}_1} = 8\mathsf{Pe}^{-1/2}$.

In the second scenario, we consider the situation with strong imposed stretching $\mathsf{Da}^{-1} > \mathsf{Pe}^{-1}$. In this scenario, we still expect to have two transitions. The first transition will be from the kinetics-limited regime to the intermediate coupled stretching enhanced mixing and kinetics limited regime while the second transition will be from this intermediate regime to the long time shear-enhanced mixing regime with no kinetics limitation. At the first transition time, we must have an equality of the masses of product determined in the two regimes $\frac{\mathsf{Da}}{4}t^{3/2} = \frac{\mathsf{PeDa}}{10\sqrt{3}}t^{5/2}$, which yields a dimensionless transition time $t_{\mathsf{Pe}_2} = \frac{1}{\mathsf{Pe}}\frac{5\sqrt{3}}{2}$; at this time the mass of the product is found out to be $m_{c,\mathsf{Pe}_2} = \frac{\mathsf{Da}}{\mathsf{Pe}^{3/2}}\frac{1}{4}\left(\frac{5\sqrt{3}}{2}\right)^{3/2}$. Similarly, at the second transition, we have $\mathsf{PeDa}\frac{t^{5/2}}{10\sqrt{3}} = 8\mathsf{Pe}t^{3/2}$. The resulting characteristic transition time is $t_{\mathsf{Da}_2} = \frac{1}{\mathsf{Da}}80\sqrt{3}$, corresponding to a mass of product at the dimensionless transition given by $m_{c,\mathsf{Da}_2} = 8\frac{\mathsf{Pe}}{\mathsf{Da}^{3/2}}(80\sqrt{3})^{3/2}$.

4. Temporal dynamics of the reactive mixing scale

We now consider the temporal behavior of the reactive mixing scale s_r, which characterizes the spatial extent of the zone where reactions take place (equation (16)). The mixing of two separated reactants creates a hotspot of reaction at the interface, which may be highly localized in space. This can be due to i) slow diffusion, ii) fast reactions, which implies that reactants are immediately consumed as they interpenetrate each other, and iii) compression of the interface due to shear deformation. In the following, we quantify the interplay of these different processes that determines the evolution of the reactive mixing scale.

4.1. Dynamics of the reactive mixing scale in the absence of shear flow

For the scenario where there is no imposed velocity gradient, the evolution of the reactive mixing scale at sufficiently long times has been mathematically demonstrated earlier [27]. For completeness, we mention it here. It was seen in 3.1.1 that the initial scaling of the reactive mixing scale, for $t < \mathsf{Da}^{-1}$, is expected to be diffusion controlled since reactions are too slow to affect the diffusive growth of the interpenetration

zone of the two reactants, resulting in

$$s_r \sim \sqrt{t}. \tag{47}$$

After this first regime, for $t > \mathsf{Da}^{-1}$, reactions can be considered to be fast compared to the observation time. Hence, the progression of the reactive mixing scale is impeded by consumption of the diffusive reactants. Therefore it evolves at a much slower rate. The temporal scaling of the reactive mixing scale can be estimated by considering the form of the reaction rate in equation (40), which follows a scaling form $R = h(t)f(x/t^{1/6})$. In this case, the similarity variable is $x/t^{1/6}$ and the reactive mixing scale, defined by the second moment of R in equation (16), is expected to follow a scaling [27]

$$s_r \sim t^{1/6}. \tag{48}$$

4.2. Reactive mixing scale dynamics with imposed flow: strong stretching regime, $\mathsf{Pe}^{-1} < \mathsf{Da}^{-1}$

In the scenario of strong stretching, we focus on times larger than Pe^{-1} because before this characteristic time the reactive mixing scale is expected to be diffusion controlled, a case which has been discussed above. For times $t < \mathsf{Da}^{-1}$, reaction can be considered to be too slow to affect the progression of the reactive mixing scale. Hence, we can apply the same approximation as in the above case but in the $z - \theta$ coordinates, which account for shear deformation. In analogy to equation (47), the reactive mixing scale is expected to grow as $z_r \sim \sqrt{\theta}$ (diffusion-limited growth) where z_r denotes the reactive mixing scale in the $z - \theta$ coordinates (we recall that $z = x'/\delta$). Therefore, the reactive mixing scale in the x' coordinate is

$$s_r \sim \delta\sqrt{\theta}\ . \tag{49}$$

We utilize the above functional relationship to arrive at a governing equation for the width. Therefore, we differentiate this with respect to time, t, to obtain

$$\frac{1}{s_r}\frac{\partial s_r}{\partial t} = \frac{1}{\delta}\frac{\partial \delta}{\partial t} + \frac{1}{2s_r^2}\ . \tag{50}$$

The above equation governs the compression and diffusion of a front for the case of strong stretching at times $t < \mathsf{Da}^{-1}$. For $t > \mathsf{Da}^{-1}$, the expected scaling is the same as discussed in the previous section at long times (equation (48)).

Note that equation (50) is the same as for the conservative mixing scale [60, 66], which is consistent with the fact that reactions are to slow to affect the progression of the front in this regime. Qualitatively, the first term depicts the compression of the reactive mixing scale due to the axial stretching and the associated perpendicular compression. On the other hand, the second term depicts the increase in the reactive mixing scale due to diffusion broadening at times where the reaction is occurring. The balance of these two terms is reached at the mixing time [52, 54]. Before the mixing time, compression is expected to dominate over diffusion, while the opposite situation develops after the mixing time for linear shear flows. The mixing

time can be estimated by recalling that we must have, at the transition, the balance between the width compression (the first term on the right hand side of equation (50)) and the diffusive growth (the second term on the right hand side of equation (50)). In the compression regime, the width of the reaction zone is given by the solution of $\frac{1}{s_r}\frac{\partial s_r}{\partial t} \sim \frac{1}{\delta}\frac{d\delta}{dt}$. which trivially yields the solution as $s_r \sim \delta$. We may thus write $\frac{1}{\delta}\frac{d\delta}{dt} \sim \frac{1}{2\delta^2}$ (where we have utilized the fact that $s_r \sim \delta$ at the transition). Simplifying this, we obtain the mixing time as $t_m \sim Pe^{-2/3}$ [60].

In summary, in the compression regime, $\mathsf{Pe}^{-1} < t < \mathsf{Pe}^{-2/3}$, the reactive mixing scale is expected to evolve by compression as $s_r \sim \frac{s_0}{\sqrt{1+\mathsf{Pe}^2 t^2}}$. In the diffusion regime, $\mathsf{Pe}^{-2/3} < t < \mathsf{Da}^{-1}$, it is expected to grow diffusively as $s_r \sim \sqrt{t}$. For $t > \mathsf{Da}^{-1}$, the progression of the reactive mixing scale is expected to be impeded by the consumption of reactants as described in the previous section and the mixing scale is expected to grow as $s_r \sim t^{1/6}$.

4.3. Reactive mixing scale dynamics with imposed flow: weak stretching, $\mathsf{Da}^{-1} < \mathsf{Pe}^{-1}$

We now consider the weak stretching scenario, for which the reaction time scale t_{Da_1} is reached earlier than the characteristic stretching time scale, t_{Pe_1}. To derive the temporal scaling of the reactive mixing scale in this regime, we appeal to the long time solution of equation (36), which can be expressed as,

$$g \sim f(t) Ai\left(\frac{x' \mathsf{Da}^{1/3}}{\delta(1+\mathsf{Pe}^2 t^2)^{1/3}\sqrt{\pi\theta}^{1/3}}\right). \tag{51}$$

where $f(t)$ is a function that depends only on time. Similarly to equation (31), this leads to a general form of the reaction rate, such as,

$$R = \mathsf{Da}\frac{x'}{t^{1/2}} g \sim h(t)\frac{x'}{s_r} Ai\left(C\frac{x'}{s_r}\right) \tag{52}$$

where $h(t)$ is a function that depends only on time, C is a constant, so that the functional form of the reaction width may be written as

$$s_r \sim \delta(1+\mathsf{Pe}^2 t^2)^{1/3}\theta^{1/6} \tag{53}$$

Upon taking the log and differentiating equation (53), we obtain

$$\frac{1}{s_r}\frac{\partial s_r}{\partial t} = \frac{1}{\delta}\frac{\partial \delta}{\partial t} - \frac{2}{3}\frac{\mathsf{Pe}^2 t}{(1+\mathsf{Pe}^2 t^2)} + \frac{1}{6\theta}\frac{d\theta}{dt} \tag{54}$$

Thus, noting that $\frac{1}{\delta}\frac{d\delta}{dt} = \frac{\mathsf{Pe}^2 t}{1+\mathsf{Pe}^2 t^2}$, $\frac{d\theta}{dt} = 1/\delta^2$ and writing θ as a function of s_r through equation (53), we obtain the compression-diffusion equation in the case of weak stretching as

$$\frac{1}{s_r}\frac{\partial s_r}{\partial t} = \frac{1}{3\delta}\frac{\partial \delta}{\partial t} + \frac{(1+\mathsf{Pe}^2 t^2)^{2/3}}{6(t+1/3\mathsf{Pe}^2 t^3)^{2/3} s_r^2} \tag{55}$$

The compressive term on the right hand side of this equation is weak as compared to the diffusive expansion (as seen from the prefactor of $\frac{1}{3}$ in equation (55)) which is absent in equation (50).

We must also reiterate that the derivation shown above is strictly speaking true for the long time behaviour (since we have appealed to the long time Airy function behavior for the concentration perturbation). This leads asymptotically to the $s_r \sim t^{1/6}$ behavior. Moreover, we shall see through the numerical results that at early times, the reaction width is completely governed by the compression term $\frac{1}{\delta}\frac{d\delta}{dt}$ seen in equation (50). Essentially it means that the first term appearing through the long time analysis scenario of the compression-diffusion equation (55) does not play any role in determining the reaction mixing scale. Rather, in the initial moments, it is simply governed by the differential equation

$$\frac{1}{s_r}\frac{\partial s_r}{\partial t} = \frac{1}{\delta}\frac{\partial \delta}{\partial t} \tag{56}$$

For completeness, we still attempt to evaluate the mixing time for this scenario for which $\frac{1}{3\delta}\frac{\partial \delta}{\partial t} \sim \frac{(1+\mathsf{Pe}^2 t^2)^{2/3}}{6\theta^{2/3}s_r^2}$. Upon substituting the form of $s_r \sim \delta^{1/3}$ in the compression regime and equating these two terms we obtain $t_m \sim \mathsf{Pe}^{-2/3}$, which is the same as for the strong stretching regime.

The expressions derived here provide governing equations for the reactive mixing scale that allow quantifying the spatial localization of chemically reactive zone across mixing fronts. While equation (50) is the same as for the conservative mixing scale, equation (55) is different, which quantifies the limitation of the growth of the mixing scale by the consumption of reactant through chemical reactions. Regardless of the regimes described in section 4.3 and 4.2, the mixing time is always equal to $\mathsf{Pe}^{-2/3}$, which is the same as for conservative mixing.

The dilution index quantifies the rate of mixing of a conservative scalar and has been utilized in recent times for the quantification of shear-induced-dilution [79]. In this regard, we may utilize the results obtained from the lamella approach to determine the dilution index. In Appendix C, we have depicted how the principles described herein may be employed to do so. As is proven, the minimum dilution occurs at a mixing time that is identical to that obtained in the preceding paragraph.

5. Numerical simulation of equations in the Lagrangian frame

In order to test the analytical expressions derived for the mass of product formed and the reactive mixing scale, we solve the set of equations (13) by means of a Chebyshev spectral collocation method [92]. This methodology has been employed in recent times to address a large assortment of nonlinear PDEs. Towards its implementation, we have to note that the domain is rescaled by L, where L is chosen sufficiently large over the desired observation time so as to prevent the boundary effects to affect the system evolution for the time span of interest. We denote the rescaled spatial variable as $\hat{z} = z/L$. The governing equations are subjected to the initial condition for a as $a(\hat{z}, 0) = 1 \ \forall \hat{z} \in (0, 1)$ and 0 otherwise. The initial condition for b is given by $b(\hat{z}, 0) = 1 - a(\hat{z}, 0)$ while for the species c we have the initial condition as $c(\hat{z}, 0) = 0$ everywhere. The boundary conditions are $a(1, \theta) = 0$, $a(-1, \theta) = 1$, $b(1, \theta) = 1$, $b(-1, \theta) = 0$ and $c(\pm 1, \theta) = 0$. The method

involves discretizing the 1D domain into the *Gauss-Lobatto* discretized grids represented by $\hat{z}_i = \cos(i\pi/N)$, where N represents the total number of intervals chosen for the solution. We make use of the Chebyshev differentiation matrices to represent the spatial derivatives. In a time discrete form (with the superscript k denoting the k^{th} time level), the discretized equation for the species a may be represented as

$$\frac{a^{k+1} - a^k}{\Delta\theta} = [a_{xx}]^{k+1} - \mathsf{Da}\, a^k b^k \left(\delta^k\right)^2 \tag{57}$$

We may obtain the time-discrete equations for the evolution of species b and c along similar lines. Briefly speaking, the governing equations for the three species are expanded in the form of n Chebyshev polynomials of the first kind over the discretized domain $\hat{z}$ as

$$a(\hat{z}) \approx \sum_{l=0}^{n} A_l T_l(\hat{z}) \tag{58}$$

We may write the discretized form of the reaction-diffusion equations as

$$\begin{aligned}
a_i^{k+1} + \Delta\theta\,[a_{xx}]_i^{k+1} &= a_i^k - \mathsf{Da}\, a_i^k b_i^k \frac{1}{1 + \mathsf{Pe}^2 (t^{k+1})^2} \\
b_i^{k+1} + \Delta\theta\,[b_{xx}]_i^{k+1} &= b_i^k - \mathsf{Da}\, a_i^k b_i^k \frac{1}{1 + \mathsf{Pe}^2 (t^{k+1})^2} \\
c_i^{k+1} + \Delta\theta\,[c_{xx}]_i^{k+1} &= c_i^k + \mathsf{Da}\, a_i^k b_i^k \frac{1}{1 + \mathsf{Pe}^2 (t^{k+1})^2}
\end{aligned} \tag{59}$$

where the subscript i represents the value of the variable at the $i-th$ node while the superscript k denotes the $k-th$ time step. The initial and boundary conditions for equation (59) may be written as

$$\begin{aligned}
&a_i^0 = 1 \;\; \forall x > 0, b_i^0 = 1 - a_i^0, c_i^0 = 0 \\
&a_N^k = 1,\; a_0^k = 0,\; b_N^k = 1,\; b_0^k = 0, c_N^k = 0,\; c_0^k = 0 \quad .
\end{aligned} \tag{60}$$

The spatial derivatives are represented by means of the Chebyshev differentiation matrices, $\mathcal{D}$, with $(\mathcal{D}\; a)$ representing the first derivative of the vector a, $(\mathcal{D}^2\; a)$ representing the second derivative of the vector a and so on. The boundary conditions of the discretized domains are incorporated by altering the first and last rows of the pertinent differentiation matrix, respectively. The MATLAB files for obtaining the spatiotemporal evolution of the concentration profiles and other derived parameters can be made available upon request. In the appendix we have demonstrated the validity of the numerical methodology presented here against full 2D simulations performed in the finite element framework of COMSOL Multiphysics. It may be seen from the figures that the simulations are in excellent agreement. The methodology presented here requires modest computational resources in comparison to the full 2D simulations [92]. In the following, we use this $1D$ numerical model of diffusion, compression and reaction in the direction transverse to the front to explore the space of Pe and Da and validate the analytical expressions derived in the previous section.

6. Discussion

In this section we shall attempt to shed light on the temporal scaling of the mass produced and trends observed for the transition times among the different regimes as obtained from the theoretical discussion in this work, and compare it against the numerical results obtained by means of the 1D Chebyshev spectral collocation method. We shall first focus on the cases of no imposed flow and imposed flow (with the two subcases of weak stretching and strong stretching). We then proceed to study the temporal evolution of the reactive mixing scale for the cases of no shear and shear while attempting to quantify the observed temporal evolutions by means of the compression-diffusion equation proposed in section 4.

6.1. Temporal evolution of the mass of product

6.1.1. No shear scenario

For completeness, we first depict the temporal evolution of the mass of product for the case where there is no imposed flow. In figure 3(a) we depict the temporal variation of the mass of the product formed for different Damköhler numbers (Da =0.1, 1, 10, 100). We observe from figure 3(a) that the initial scaling obtained from the numerical simulation does corroborate excellently with the theoretical predictions made in section 3.1.1; in the initial reaction-diffusion regime (reaction kinetics dominated regime), the mass scales as $m_c \sim \mathsf{Da} t^{3/2}$, as predicted analytically. Essentially we observe that as Da increases, there is a concomitant increase in the product mass produced. Beyond the transition time $t_{\mathsf{Da}_1} = 32/\mathsf{Da}$ the mass scaling is no more limited by reaction kinetics and evolves as per the scaling $m_c \sim t^{1/2}$, corresponding to the diffusion-limited regime, as theoretically obtained in section 3.1.2. In accordance to the theoretical predictions, it is seen from figure 3(a) that beyond the time t_{Da_1}, m_c becomes independent of the Damköhler number. Clearly, this underpins the fact that beyond the transition time, the evolution is limited by diffusion and not dictated by the reaction kinetics term. In figure 3(b), we depict the temporal evolution of the rescaled mass of the product $m_c/m_{c,\mathsf{Da}_1}$ as a function of the rescaled time t/t_{Da_1}. The curves depicted in figure 3(a) collapse on top of each other, thus confirming the validity of the theoretical predictions of the rescaling of the transition time and the mass of the product formed at that particular transition time.

6.1.2. Weak stretching scenario

We now proceed to analyze the weak stretching scenario $\mathsf{Da}^{-1} < \mathsf{Pe}^{-1}$. In figure 4 we depict the temporal evolution of the mass of the product formed for $\mathsf{Pe} = 0.1$ and $\mathsf{Da} = 0.1, 1, 10, 100$. Initially all the curves increase as per the scaling $m_c \sim t^{3/2}$, indicating the kinetics-limited regime. After this initial scaling, depending on the magnitude of Da, a transition from the $m_c \sim t^{3/2}$ scaling to the $m_c \sim t^{1/2}$ scaling is observed. The dependence of the transition time on Da is consistent with the predicted relationship $t \sim \mathsf{Da}^{-1}$. Then at around $t \sim \mathsf{Pe}^{-1}$ all the curves merge together to follow a mass scaling in the form $t^{3/2}$, which is consistent with the expected shear-enhanced reactive mixing regime. For the case $\mathsf{Da} = \mathsf{Pe} = 0.1$,

(a)

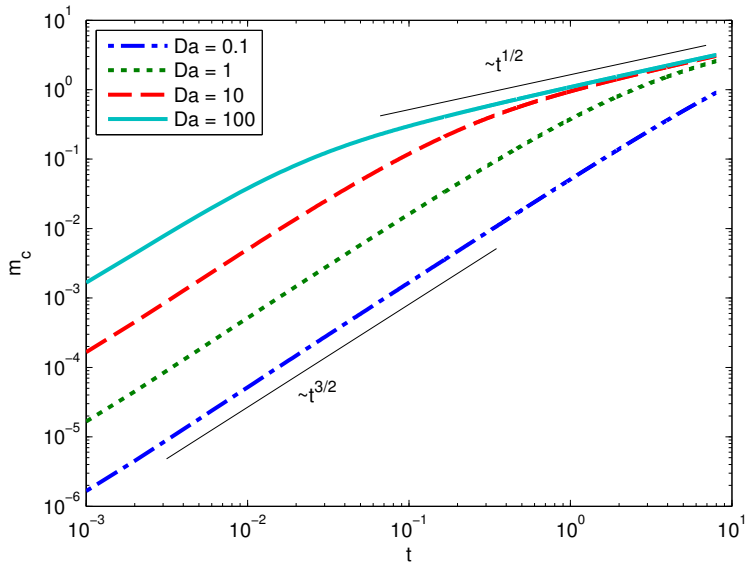

(b)

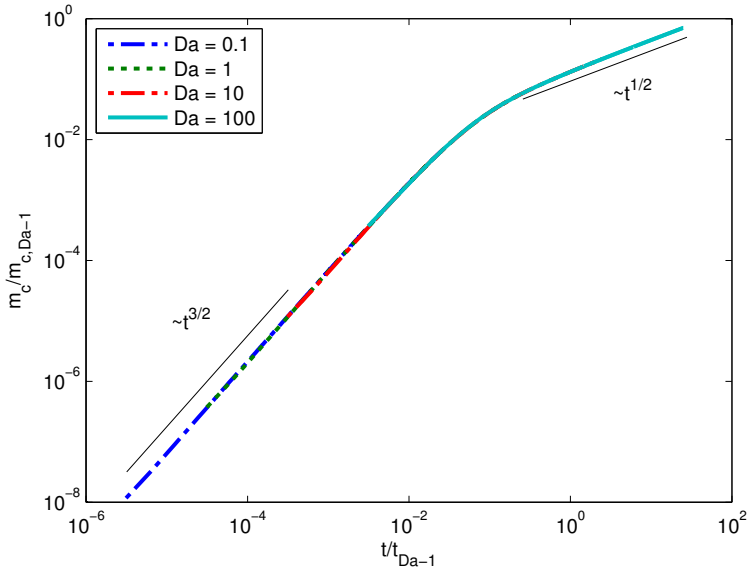

Figure 3: (a) Temporal evolution of the mass of product formed for $\mathsf{Da} = 0.1, 1, 10, 100$ in the case where $\mathsf{Pe} = 0$, as obtained from the Chebyshev spectral method. (b) Rescaled temporal evolution of the mass of product formed for $\mathsf{Da} = 0.1, 1, 10, 100$ for the case where there is no externally imposed flow. Towards rescaling the aforementioned variables, the time has been rescaled as $t/(32/\mathsf{Da})$ while the mass has been rescaled as $m_c/(45/\sqrt{\mathsf{Da}})$.

the intermediate regime does not exist and the system transits directly from the kinetics limited regime to the long-time shear-enhanced reactive mixing regime (wherein both the regimes have a temporal scaling of $m_c \sim t^{3/2}$). Besides this, we also notice that, in accordance to the theoretical prediction, the long time

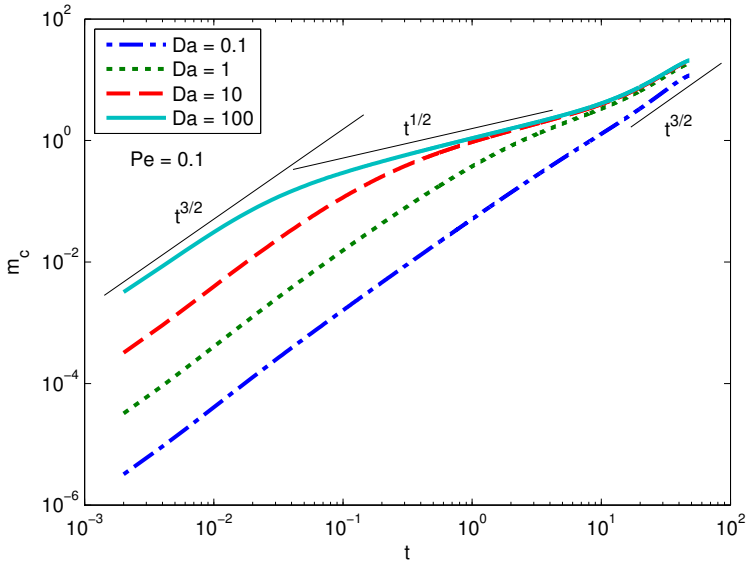

Figure 4: Temporal evolution of the product mass for $\mathsf{Pe} = 0.1$ for $\mathsf{Da} = 0.1, 1, 10, 100$. The three distinct regimes, reaction controlled, diffusion controlled and stretching controlled, are observed when the two transition times are separated (i.e. $\mathsf{Pe} < \mathsf{Da}$). As Pe becomes comparable to Da, the intermediate regime of diffusion-limited growth is not observed.

behavior of m_c is independent of Da. Upon rescaling the curves of figure 4 by the first transition time $t_{\mathsf{Da}_1} = 32/\mathsf{Da}$ for the time axis, and the mass of product at this time $m_{c,\mathsf{Da}_1} \approx 45/\sqrt{\mathsf{Da}}$, they collapse into each other (figure 5(a)) for the first two regimes (i.e. for $t < t_{\mathsf{Pe}_1}$). This confirms the validity of the predicted scalings for the first transition time t_{Da_1}. In figure 5(b) we observe that the curves for different Pe (and different Da as well) collapse onto each other for the later two regimes (i.e. for $t > t_{\mathsf{Da}_1}$) when we rescale time for the the curves in figure 4 by the second transition time $t_{\mathsf{Pe}_1} \approx \mathsf{Pe}^{-1}$ and the mass of the product formed by $m_c \approx 8\mathsf{Pe}^{-1/2}$.

We remark that all the observations are in complete agreement with the theoretical predictions presented in section 3. The regime $\mathsf{Da}^{-1} < \mathsf{Pe}^{-1}$ thus essentially decouples the effect of stretching, active for $t > \mathsf{Pe}^{-1}$, from the effect of kinetics limitations, which are significant for $t < \mathsf{Da}^{-1}$. In what follows, we shall consider the case where the fluid stretching is coupled to the chemical reactions, i.e. the strong stretching scenario where $\mathsf{Pe}^{-1} < \mathsf{Da}^{-1}$.

6.1.3. Strong stretching scenario

In figure 6(a) we investigate the strong stretching scenario $\mathsf{Pe}^{-1} < \mathsf{Da}^{-1}$. We consider the temporal evolution of m_c for the cases where $\mathsf{Pe} = 100$ and $\mathsf{Da} = 0.1, 1, 10, 100$. For $t < Pe^{-1}$, we observe that the evolution of m_c scales as $m_c \sim t^{3/2}$. After this dimensionless time, stretching becomes significant while reaction kinetics is still a limiting factor since $t < \mathsf{Da}^{-1}$. Hence, in this intermediate regime we

(a)

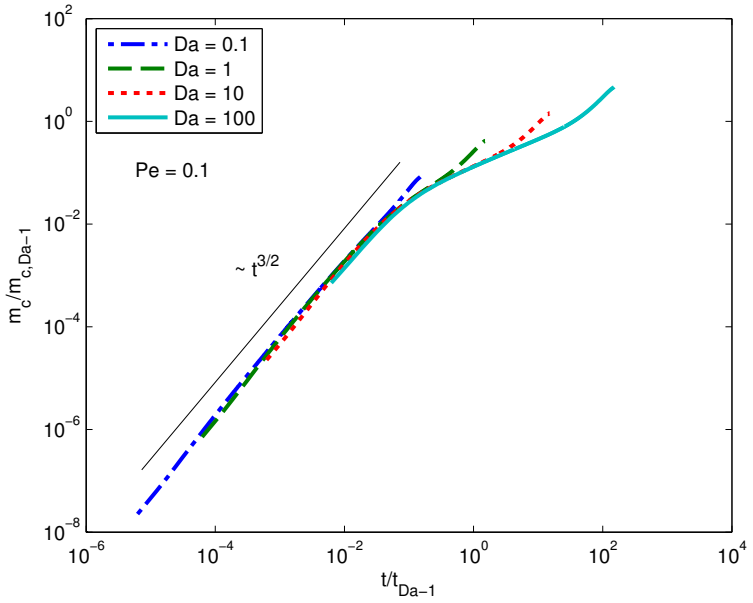

(b)

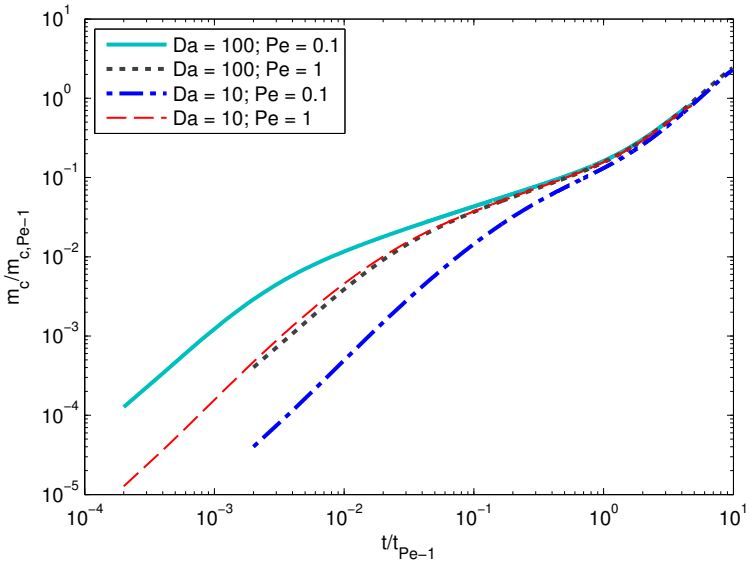

Figure 5: (a) Scaled mass of product vs time $m_c/m_{c,\mathsf{Da}_1}$ as a function of t/t_{Da_1}, for $\mathsf{Pe} = 0.1$ and $\mathsf{Da} = 0.1, 1, 10, 100$ at the first transition time for weak stretching, t_{Da_1}. (b) Scaled mass of product vs time, for $\mathsf{Pe} = 0.1$ and $\mathsf{Pe} = 1$ for $\mathsf{Da} = 10, 100$ at the second transition time for weak stretching, t_{Pe_1}.

observe the predicted accelerated scaling $m_c \sim t^{5/2}$, induced by the coupling between kinetics limitation and stretching. This first transition is confirmed by rescaling time by $t_{\mathsf{Pe}_2} = 5\sqrt{3}\mathsf{Pe}^{-1}/2$ and mass by $m_{c,\mathsf{Pe}_2} = (5\sqrt{3}/2)^{3/2}/\mathsf{Pe}^{3/2}$, which collapses the curves together (please refer to figure 7 (a)). The second

(a)

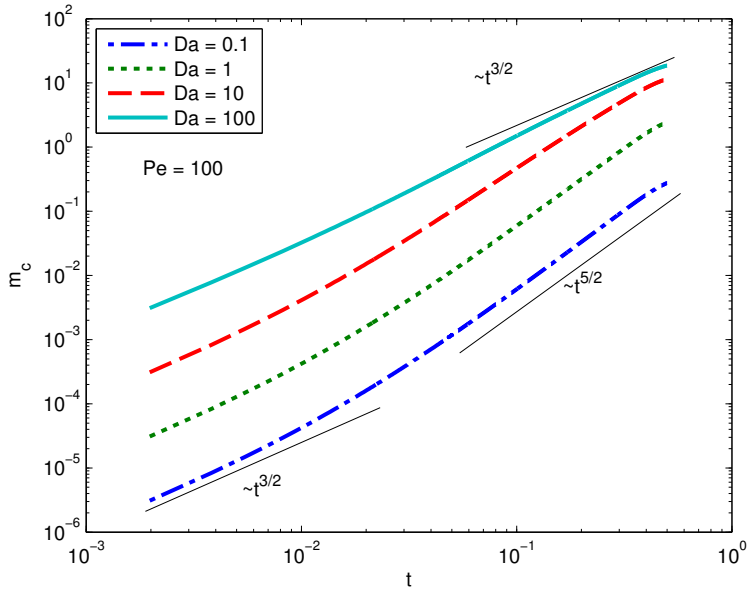

(b)

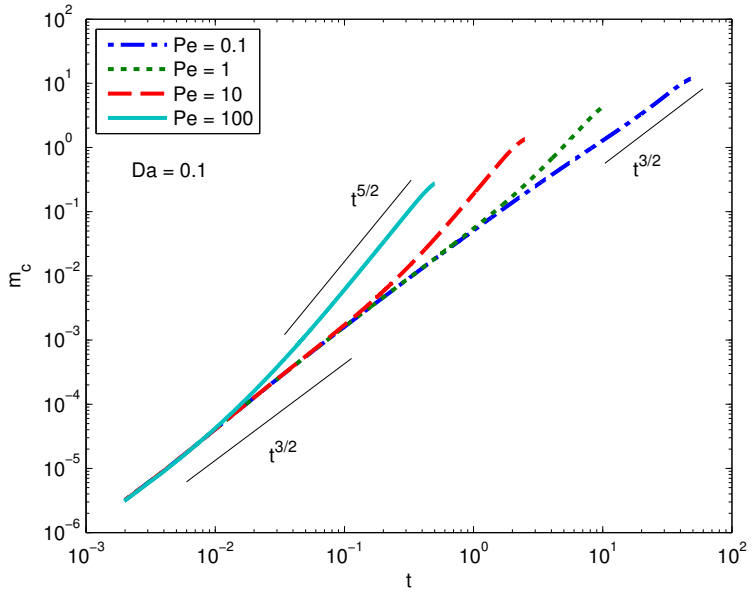

Figure 6: (a) Temporal evolution of the product mass for $\mathsf{Pe} = 100$ and $\mathsf{Da} = 0.1, 1, 10, 100$. As opposed to the case considered in figure 4, we consider the effect of strong stretching, thus allowing the system to undergo the transition into the stretching controlled regime at early times. (b) Temporal evolution of the product mass for $\mathsf{Da} = 0.1$ and $\mathsf{Pe} = 100, 10, 1, 0.1$.

transition from $m_c \sim t^{5/2}$ regime to $m_c \sim t^{3/2}$ regime is not visible on a single simulation due to very long time of simulation required. This transition is however visible when collapsing the different simulations

together through rescaling time by $t_{\mathsf{Da}_2} \approx 80\sqrt{3}/\mathsf{Da}$ and mass by $m_{c,\mathsf{Da}_2} \approx 8(80\sqrt{3})^{3/2}\mathsf{Pe}/\mathsf{Da}^{3/2}$ (figure 7(b)).

Note that the intermediate scaling is not observed for $\mathsf{Pe} = \mathsf{Da} = 100$, since the system transitions directly from the early time kinetics-limited regime with no significant stretching to the stretching enhanced reactive mixing regime with no kinetics limitation, which both scale as $m_c \sim t^{3/2}$. The agreement with theoretical derivations is further confirmed by the series of simulations performed for $\mathsf{Da} = 0.1$ and $\mathsf{Pe} = 0.1, 1, 10, 100$ (figure 6(b)). The transition t_{Pe_2} is readily seen in this case when considering the trends of the transition from the $m_c \sim t^{3/2}$ regime to the $m_c \sim t^{5/2}$ regime as Pe is increased. For the situation for which $\mathsf{Da} \sim \mathsf{Pe}$, we see again that the region in which there is a coupling of the reaction kinetics and stretching vanishes as expected. Figure 7(a) clearly depicts that when the time and the mass of the product are rescaled by t_{Pe_2} and m_{c,Pe_2} respectively, we observe that the curves in figure 6(b) collapse onto each other for the first two regimes (i.e. for $t < \mathsf{Da}^{-1}$). On the other hand figure 7(b) clearly depicts that when the time and the mass of the product are rescaled by t_{Da_2} and m_{c,Da_2}, we obtain a good collapse of the curves depicted in figure 6(a) for the other later two regimes (i.e. for $t > \mathsf{Pe}^{-1}$).

6.2. Temporal evolution of the reactive mixing scale

In figure 8 we depict the temporal evolution of the reactive mixing scale, s_r as a function of time for configurations of strong stretching as manifested through a low Damköhler ($\mathsf{Da} = 0.1$) and a Péclet that is larger than the Damköhler ($\mathsf{Pe} = 0.1, 1, 10, 100$). We observe a good agreement with the compression-diffusion equation elucidated in section 4.2. There is an initial diffusion controlled growth of the reactive mixing scale until the time Pe^{-1}. After this time we observe a compression (the reactive mixing scale decreases), followed by a transition at $t \sim \mathsf{Pe}^{-2/3}$ to the $s_r \sim t^{1/2}$ regime.

In figure 9 we depict the evolution of the reactive mixing scale as a function of time for configurations of weak stretching with $\mathsf{Da} = 100$ and $\mathsf{Pe} = 0.1, 1, 10, 100$. It may be observed from figure 9 that at small times the reactive mixing scale grows at a rate which is limited by diffusion until the time $t \sim \mathsf{Pe}^{-1}$ at which a compression occurs in the system. This is most prominently seen in the case of $\mathsf{Pe} = 100$ and $\mathsf{Pe} = 10$. In between the stretching time Pe^{-1} and and the mixing time $\mathsf{Pe}^{-2/3}$ we observe that the impact of the stretching is to compress the reactive mixing scale. This compression occurs until the mixing time $t_m \sim \mathsf{Pe}^{-2/3}$, beyond which we observe a growth of the reactive mixing scale as $s_r \sim t^{1/6}$. The latter is expected since the dimensionless time is larger than the Da^{-1} and hence the expansion of the reaction mixing scale is impeded by the rate of consumption of the reactants. The solution of equation (55) is seen to be valid after the reactive mixing time. However it is unable to predict the observed compression. This may be attributed to the fact that equation (55) is derived by taking into consideration the scaling form at large times (please refer to section 4.3). It is however observed that the compression-diffusion equation (equation (50), derived in section 4.2) is able to predict the early time behavior for the curves to a good

(a)

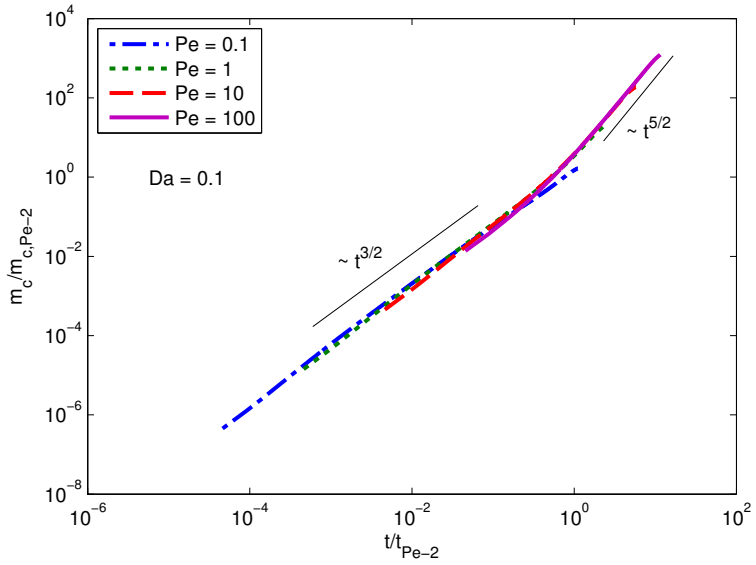

(b)

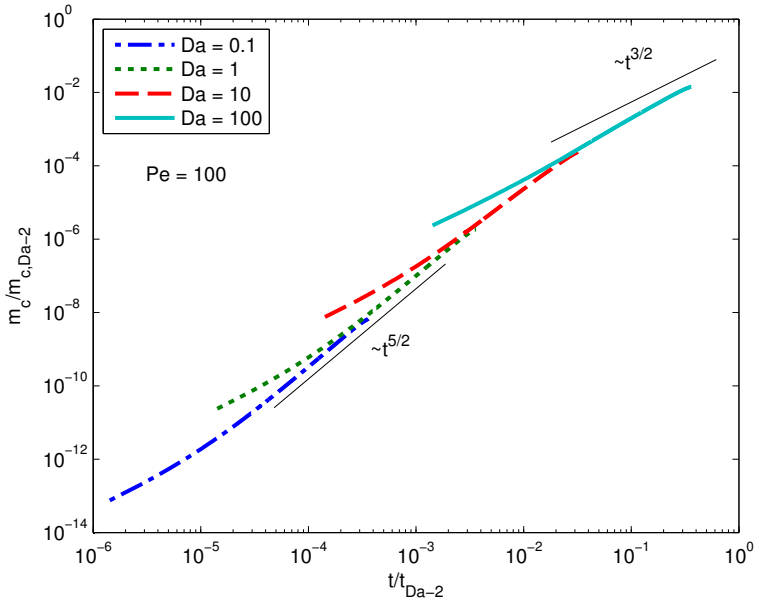

Figure 7: (a) Rescaled mass of product, $m_c/m_{c,\mathsf{Pe}_2}$, vs rescaled time, t/t_{Pe_2}, for $\mathsf{Da} = 0.1$ (strong stretching) and $\mathsf{Pe} = 0.1, 1, 10, 100$ at the first transition time, t_{Pe_2}. (b) Rescaled mass of product, $m_c/m_{c,Da_2}$, vs rescaled time, t/t_{Da_2}, for $\mathsf{Pe} = 100$ (strong stretching) and $\mathsf{Da} = 0.1, 1, 10, 100$ at the second transition time, t_{Da_2}.

approximation. Consequently, this observation suggests that the chemical reactions do not affect the early time behavior of the reactive mixing scale.

Moving beyond the extreme cases of Pe and Da in figure 10 we represent the temporal evolution of the

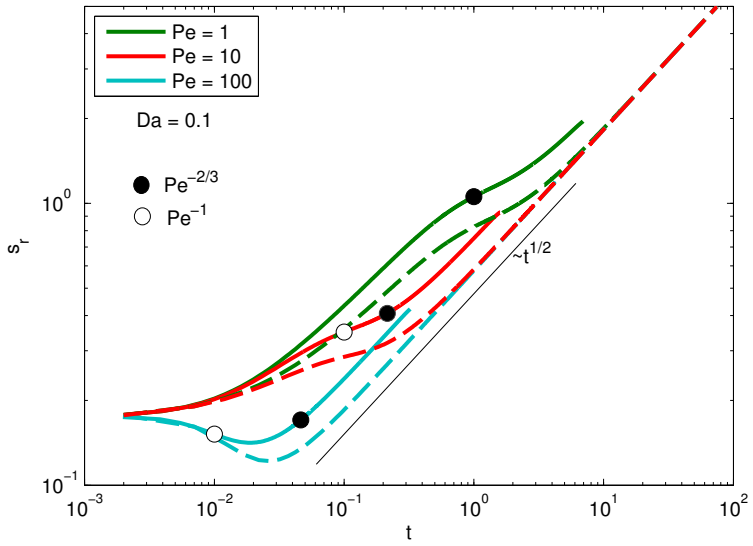

Figure 8: Temporal evolution of the reactive mixing scale for a case for which Pe is larger than Da. We have chosen Da $= 0.1$ and depicted the reactive mixing scales for Pe $= 1, 10, 100$. The black filled markers corresponds to the mixing time $t_m = \mathsf{Pe}^{-2/3}$ while the white filled marker corresponds to the time Pe^{-1} for Pe $= 10$ and 100. The solid lines represent the solution from the 1D Chebyshev spectral collocation method while the dashed lines represent the prediction from the compression diffusion equation (50)

reactive mixing scale for a situation where Pe and Da are moderate and not much different from each other in a hope to outline the transition from one kind of behavior to the other kind of behavior. For this case we have chosen Da $= 10$ and Pe $= 1$. The solid line represents the numerical solution while the dash-dot line represents the solution obtained from equation (50) while the dashed line represents the solution obtained from equation (55). It may be clearly observed that the initial evolution of the reactive mixing scale is reasonably predicted by equation (50) while beyond the overlap of the two curves, the curve is depicted in a better fashion by (55). The crossover in behavior occurs at the the mixing time scale, which in this case is close to 1.

7. Conclusions

This study provides analytical expressions of upscaled effective reaction rates in the presence of shear flow. These expressions quantify the coupling between mixing limitations, governed by fluid stretching and diffusion and quantified by the Péclet number, and kinetic limitations, quantified by the Damköhler number. It is seen that velocity gradients promote mixing by elongating the interface available for diffusive mass transfer and increasing concentration gradients. As discussed in this study, the coupling of this phenomenon with a broad range of characteristic reaction time scales is non-trivial. We have thus quantified the impact

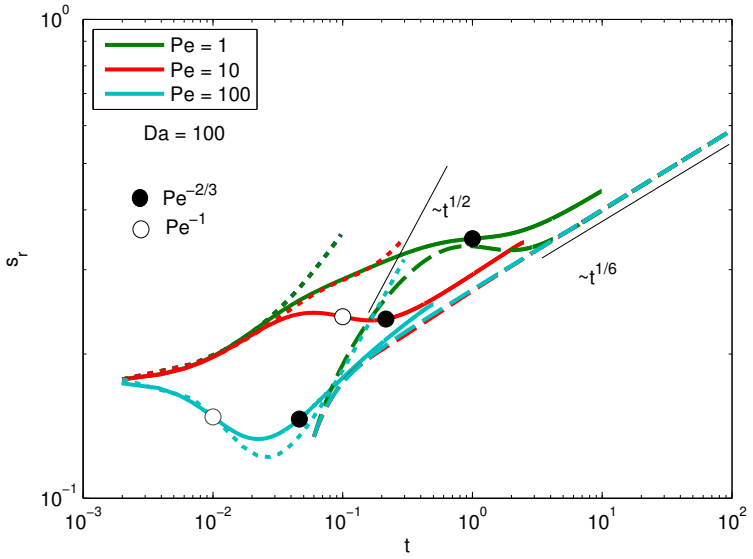

Figure 9: Temporal evolution of the reactive mixing scale as a function of time for $\mathsf{Da} = 100$ and $\mathsf{Pe} = 1, 10, 100$. The black filled markers correspond to the mixing time $t \sim \mathsf{Pe}^{-2/3}$ while the white filled marker correspond to the time Pe^{-1} for the cases $\mathsf{Pe} = 10$ and 100. The solid lines represent the numerical solution obtained using the 1D Chebyshev spectral collocation method, the dotted lines represent the solution obtained from the compression-diffusion equation in section 4.2, and the dashed curves represent the curves obtained using the compression-diffusion equation in section 4.3.

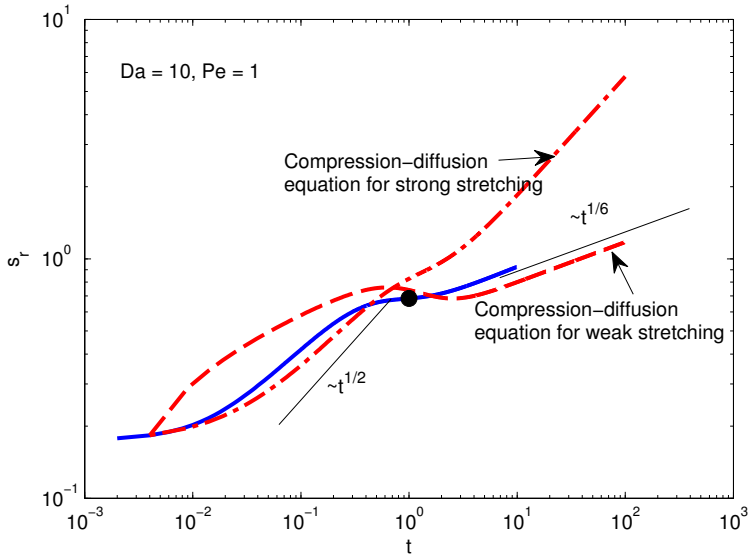

Figure 10: Temporal evolution of the reactive mixing scale as a function of time for the case with $\mathsf{Da} = 10$ and $\mathsf{Pe} = 1$. The solid line represents the solution obtained from the 1D Chebyshev spectral collocation method. The dashed and the dash-dot-dash line represent the solutions from the compression diffusion equations (55) and (50), respectively.

of the Damköhler and Péclet numbers on the effective reaction kinetics of mixing front subject to shear deformation. Different regimes have been identified theoretically in this temporal behavior, as well as the transition times between them. Through the functional dependency of the reactive mixing scale on time, we have analyzed the spatial localization of reactivity as a function of time, Damköhler and Péclet numbers. We have also proposed an efficient and fast numerical scheme based on a Chebyshev spectral collocation method in order to tackle the nonlinear reaction-advection-diffusion problem numerically, which has allowed us to verify successfully all our theoretical predictions.

While previous works had mostly focused on the cases of $\mathsf{Pe} = 0$ with variable Da or $\mathsf{Da} = \infty$ with variable Pe, the theoretical framework presented here spans the full space of Pe and Da (see figure 2). In the case of a stretching that is weak in comparison to the reaction, i.e. for $\mathsf{Pe} < \mathsf{Da}$, the effects of kinetics limitations and mixing enhancement by shear are essentially decoupled. Kinetics limitation is dominant in the early time regime for $t < t_{\mathsf{Da}_1} = 32/\mathsf{Da}$, while stretching enhanced mixing is dominant in the late time regime $t > t_{\mathsf{Pe}_1} = 1/\mathsf{Pe}$. In the intermediate regime reactions are limited by diffusion, leading to the classical diffusive scaling. In the case of a stretching that is strong in comparison to the reaction kinetics , i.e. for $\mathsf{Pe} > \mathsf{Da}$, we have shown the existence of an intermediate regime at times $t_{\mathsf{Pe}_2} < t < t_{\mathsf{Da}_2}$, with $t_{\mathsf{Pe}_2} = \frac{1}{\mathsf{Pe}} 5\sqrt{3}/2$ and $t_{\mathsf{Da}_1} = \frac{1}{\mathsf{Da}} 80\sqrt{3}$, where stretching enhanced mixing and kinetics limitations are strongly coupled. This leads to an accelerated effective kinetics with $m_c \approx \frac{\mathsf{PeDa}}{10\sqrt{3}} t^{5/2}$.

The presence of a background velocity gradient affects the evolution of the reactive mixing scale, which defines the region around the interface between the two reactants where reaction mostly occurs. In the absence of an imposed shear, the reactive mixing scale initially grows as $s_r \sim t^{1/2}$, due to control by molecular diffusion. Beyond the time t_{Da_1} this growth slows down as $s_r \sim t^{1/6}$ due to consumption of reactants by the chemical reaction. The presence of a velocity gradient affects this evolution by introduction a regime of compression in the temporal evolution of the reactive mixing scale. We have attempted to formalize the nature of this evolution of the reactive mixing scale by introducing a compression-diffusion equation for each of the two different cases of weak and strong stretching. We have shown that the reactive layer is compressed between the characteristic stretching time $t \sim \mathsf{Pe}^{-1}$ and the mixing time $t_m \sim \mathsf{Pe}^{-2/3}$, at which diffusion balances compression. Beyond this time the reactive mixing scale evolves as $s_r \sim t^{1/6}$ in the case of weak stretching and $s_r \sim t^{1/2}$ in the case of strong stretching. The compression-diffusion equations are able to predict the nature of the evolution of the reactive mixing scale in their respective domains of validity with reasonable accuracy.

The results presented in this work represent a step towards understanding how complex stretching processes found in particular in porous media interact with the reactivity of transported solutes to determine the dynamics of upscaled effective kinetics and the degree of spatial localization of reactive hotspots. While the presented results are directly relevant to 2D porous media where linear deformation has been observed [81], they may also be extended to power law deformation [66] and exponential deformation [80]. Such

stretching dynamics may be related to topological metrics such as the Okubo-Weiss (OW) parameter [79]. The presented methodology, developed here for a constant velocity gradients, may be extended to spatially variable velocity gradients based on the lamella representation of mixing fronts. For any given flow field, we may always consider a stretched front to be comprised of a large number of small elements [54]. In this way, locally, we may address the evolution of the concentration of the species involved in the direction perpendicular to the strip (the local moving coordinate system comprises of two directions: one direction points along the lamella while the other is perpendicular to it). Based on the ideas in this work, we may thus extend this framework to account for reactions between two species encountering arbitrary flow fields.

However, we must briefly mention the drawbacks of the reactive lamella approach and accordingly mention a prospective road map for potential research. Since chemical reactions introduce strong non-linearities, we assumed that a given isolated lamella does not interact with other lamellae (note that this is not an issue for conservative mixing processes since lamella concentrations add up linearly upon overlapping). While this hypothesis is satisfied exactly for stratified flows, the same may not hold true for other flow fields, for example in situations where there is a severe bending of the material line which renders the evolution of the concentration fields in that local coordinate system to be necessarily 2D instead of 1D. For such flows, the lamella approach is expected to work best for the case of high Péclet numbers (wherein the diffusion is small compared to advection). We have assumed that the diffusion coefficients of all the species in the reaction are equal. This assumption allows us to make several analytical treatments to the reduced set of governing equations in the warped coordinates and obtain underlying scaling regimes and transition times in terms of the Péclet and Damköhler numbers. A more general formulation to study the reaction dynamics of such a system would entail relaxation of this assumption [45, 46]. In the situation where the diffusion coefficients are different, one would obtain travelling fronts which exhibit a rich range of dynamics. This can potentially form the basis for further development based on this work towards identifying the impact of diffusivity contrast on enhanced reaction kinetics in the presence of shear flows. Going beyond 2D, these ideas may be extended to 3D flows, which are inevitable when considering groundwater flow. The evolution of material volumes in 3D can occur either in the form of sheets or fingers, depending on the local flow structure (see [55] for several such situations). For the former scenario, we may apply a similar procedure for the sheets in which the direction normal to the sheets is the primary direction of species dynamics. For the later scenario, however, we may conceptualize the fingers (or equivalently tube-like structures) in a local cylindrical coordinate in which the axial direction is aligned along the direction of the strip and the radial direction is the normal direction along which the species dynamics occurs. Interestingly, one possibility is to use this framework in conjugation with information about the conductivity field of a porous media which may be related to the temporal evolution of stretching for a given material line (cf. [93]). Thus, prospects for further work include extending the numerical framework presented here to more complex stretching configurations, involving spatial and temporal fluctuations in stretching rates, as well as more complicated

reaction kinetics including multistep or higher order reactions.

8. Acknowledgments

AB would gratefully like to acknowledge postdoctoral funding through the *Agence Nationale de la Recherche* (ANR-14-CE04-0003-01 –subsurface mixing and reaction). MD acknowledges the support of the European Research Council (ERC) through the project MHetScale (617511).

Appendix A. Transformation into a moving coordinate system

We consider a linear transformation into the coordinate system moving and rotating with the material line,

$$\tilde{\mathbf{x}}' = \mathbf{A}^\top(t)\left[\tilde{\mathbf{x}} - \tilde{\mathbf{x}}(\tilde{t})\right], \qquad \frac{d\tilde{\mathbf{x}}(\tilde{t})}{dt} = \mathbf{u}[\tilde{\mathbf{x}}(\tilde{t})] \tag{A.1}$$

where $\mathbf{A}(\tilde{t})$ is an orthogonal matrix specified below in equation (A.11). Thus, concentration $\tilde{a}(\tilde{\mathbf{x}},\tilde{t})$ is given in terms of the concentration $\tilde{a}'(\tilde{\mathbf{x}},\tilde{t})$ in the moving coordinate system as

$$\tilde{a}(\tilde{\mathbf{x}},\tilde{t}) = \tilde{a}'(\mathbf{A}^\top(\tilde{t})\left[\tilde{\mathbf{x}} - \tilde{\mathbf{x}}(\tilde{t})\right],\tilde{t}), \tag{A.2}$$

and correspondingly for $\tilde{b}(\tilde{\mathbf{x}},\tilde{t})$ and $\tilde{c}(\tilde{\mathbf{x}},\tilde{t})$. Inserting (A.2) into (1) for $\tilde{a}(\tilde{\mathbf{x}},\tilde{t})$ gives

$$\frac{\partial\tilde{a}'(\tilde{\mathbf{x}}',\tilde{t})}{\partial t} + \left[\frac{d\mathbf{A}^\top(\tilde{t})}{dt}\mathbf{A}(\tilde{t})\tilde{\mathbf{x}}' - \mathbf{u}[\tilde{\mathbf{x}}(\tilde{t})]\mathbf{A}(\tilde{t})\right]\nabla'\tilde{a}'(\tilde{\mathbf{x}}',\tilde{t}) + \mathbf{u}\left[\mathbf{A}(\tilde{t})\tilde{\mathbf{x}}' + \tilde{\mathbf{x}}(\tilde{t})\right]\mathbf{A}(\tilde{t})\nabla'\tilde{a}'(\tilde{\mathbf{x}}',\tilde{t}) =$$
$$D\nabla'\cdot\mathbf{A}^\top\mathbf{A}(\tilde{t})\nabla'c'(\tilde{\mathbf{x}}',\tilde{t}) - k\tilde{a}'(\tilde{\mathbf{x}}',\tilde{t})b'(\tilde{\mathbf{x}}',\tilde{t}). \tag{A.3}$$

We note that $\mathbf{A}^\top(\tilde{t})\mathbf{A}(\tilde{t}) = 1$ due to the orthogonality of $\mathbf{A}$. Furthermore, we expand

$$\mathbf{u}\left[\mathbf{A}(\tilde{t})\tilde{\mathbf{x}}' + \tilde{\mathbf{x}}(\tilde{t})\right] = \mathbf{u}\left[\tilde{\mathbf{x}}(\tilde{t})\right] + \boldsymbol{\epsilon}(\tilde{t})\mathbf{A}(\tilde{t})\tilde{\mathbf{x}}' + \ldots, \tag{A.4}$$

where we have defined the deformation rate tensor

$$\epsilon_{ij}(\tilde{t}) = \frac{\partial u_i[\tilde{\mathbf{x}}(\tilde{t})]}{\partial\tilde{x}_j}. \tag{A.5}$$

Inserting (A.4) into (A.3) gives

$$\frac{\partial\tilde{a}'(\tilde{\mathbf{x}}',\tilde{t})}{\partial t} + \left[\frac{d\mathbf{A}^\top(\tilde{t})}{dt}\mathbf{A}(\tilde{t}) + \mathbf{A}^\top(\tilde{t})\boldsymbol{\epsilon}(\tilde{t})\mathbf{A}(\tilde{t})\right]\tilde{\mathbf{x}}'\cdot\nabla'\tilde{a}'(\tilde{\mathbf{x}}',\tilde{t}) = D\nabla'^2\tilde{a}'(\tilde{\mathbf{x}}',\tilde{t}) - k\tilde{a}'(\tilde{\mathbf{x}}',\tilde{t})b'(\tilde{\mathbf{x}}',\tilde{t}). \tag{A.6}$$

The expression in the square brackets is the deformation rate tensor $\boldsymbol{\epsilon}'(\tilde{t})$ in the moving coordinate system. As pointed out in [55], it is a pseudotensor.

For the simple shear flow $\mathbf{u}(\tilde{\mathbf{x}}) = Gy\mathbf{e}_x$ under consideration here, the deformation rate tensor is

$$\boldsymbol{\epsilon}(\tilde{t}) = \begin{pmatrix} 0 & G \\ 0 & 0 \end{pmatrix}. \tag{A.7}$$

A material strip $\tilde{\boldsymbol{\ell}}(\tilde{t})$ oriented initially perpendicular to the flow direction evolves as

$$\tilde{\boldsymbol{\ell}}(\tilde{t}) = \tilde{\ell}_0 \begin{pmatrix} G\tilde{t} \\ 1 \end{pmatrix} \tag{A.8}$$

where $\tilde{\ell}_0 = |\tilde{\boldsymbol{\ell}}(t=0)|$ is the initial elongation. The strip length $\tilde{\ell}(\tilde{t}) = |\tilde{\boldsymbol{\ell}}(\tilde{t})|$ is (please refer to figure 1)

$$\tilde{\ell}(\tilde{t}) = \tilde{\ell}_0 \sqrt{1 + (G\tilde{t})^2}. \tag{A.9}$$

Due to volume conservation, $\tilde{\ell}(\tilde{t})\tilde{\delta}(\tilde{t}) = \tilde{\ell}_0\tilde{\delta}_0$, the width of the strip is given by

$$\tilde{\delta}(\tilde{t}) = \frac{\tilde{\delta}_0}{\sqrt{1 + (G\tilde{t})^2}}. \tag{A.10}$$

We transform into the coordinate system whose x'–axis is oriented perpendicular to the material strip. Thus, the orthogonal matrix $\mathbf{A}(\tilde{t})$ is here given by

$$\mathbf{A}(\tilde{t}) = \frac{1}{\sqrt{1 + (G\tilde{t})^2}} \begin{pmatrix} 1 & G\tilde{t} \\ -G\tilde{t} & 1 \end{pmatrix} \tag{A.11}$$

So, we obtain for $\boldsymbol{\epsilon}'(\tilde{t})$ the triangular form

$$\boldsymbol{\epsilon}'(\tilde{t}) = \frac{1}{1 + (G\tilde{t})^2} \begin{pmatrix} -G^2\tilde{t} & 0 \\ G - G^3\tilde{t}^2 & G^2\tilde{t} \end{pmatrix}. \tag{A.12}$$

Initially, the concentration is uniformly distributed along the solute front, see (6), that is, in the moving coordinate system $\tilde{a}'(\tilde{\mathbf{x}}', \tilde{t}=0) = 1 - H(\tilde{x}')$ and $b'(\tilde{\mathbf{x}}', \tilde{t}=0) = H(\tilde{x}')$ with $H(\tilde{x}')$ the Heaviside step function. Due to symmetry, the species concentrations are independent of $\tilde{y}'$, this means $\tilde{a}'(\tilde{\mathbf{x}}', \tilde{t}) \equiv \tilde{a}'(\tilde{x}', \tilde{t})$ and $b'(\tilde{\mathbf{x}}', \tilde{t}) \equiv b'(\tilde{x}', \tilde{t})$. Thus, for the above initial condition, the advection-diffusion problem (A.6) accross the strip simplifies to

$$\frac{\partial \tilde{a}'(\tilde{x}', \tilde{t})}{\partial t} - \Omega(\tilde{t})\tilde{x}'\frac{\partial \tilde{a}'(\tilde{x}', \tilde{t})}{\partial \tilde{x}'} - D\frac{\partial^2 \tilde{a}'(\tilde{x}', \tilde{t})}{\partial \tilde{x}'^2} = -k\tilde{a}'(\tilde{x}', \tilde{t})b'(\tilde{x}', \tilde{t}), \tag{A.13}$$

where we have defined

$$\Omega(\tilde{t}) = \frac{G^2\tilde{t}}{1 + (G\tilde{t})^2} = \frac{1}{\tilde{\ell}(\tilde{t})}\frac{d\tilde{\ell}(\tilde{t})}{d\tilde{t}} = -\frac{1}{\tilde{\delta}(\tilde{t})}\frac{d\tilde{\delta}(\tilde{t})}{d\tilde{t}}. \tag{A.14}$$

For simplicity of notation, we drop the primes for the remainder of the paper.

Appendix B. Validation of 1D methodology

We present here a validation of the 1D Chebyshev spectral collocation method which has been employed in the present work. We compare the temporal evolution of the mass of the product formed against 2D simulations performed in the finite element framework of COMSOL Multiphysics. For the 2D simulation, we

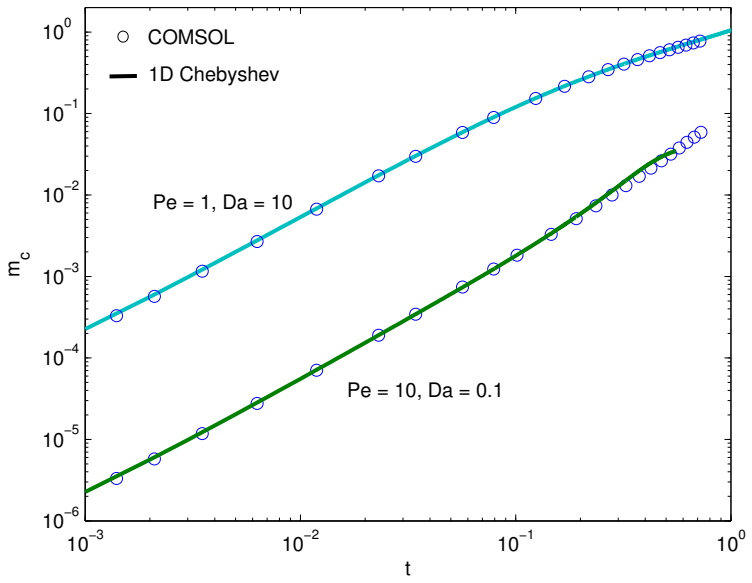

Figure B.11: Temporal evolution of the mass of product formed for two different cases: $\mathsf{Da} = 0.1, \mathsf{Pe} = 10$ and $\mathsf{Da} = 10, \mathsf{Pe} = 1$. The symbols denote the results obtained from the COMSOL 2D simulations, while the solid lines are those obtained from the 1D Chebyshev collocation method (please see 5).

consider the case of a stretching front for two different cases, $\mathsf{Da} = 0.1, \mathsf{Pe} = 10$ and $\mathsf{Da} = 10, \mathsf{Pe} = 1$. The grid spacing employed in COMSOL is 0.1 while the domain size is taken to be 20×20. Each front is chosen to be of size 10, which, compared to the nondimensional length 1 is large enough to prevent the periodic boundary condition from interacting with the diffusion front in the time of interest of our observation (we refer the reader to section 2.2 for a discussion regarding this). The minimum grid size decides the initial width of the reaction front and, consequently, the system evolution. For the 1D spectral simulation presented in figure B.11, we have employed a domain length of 30 with $N = 384$ intervals for the 1D Chebyshev spectral collocation method. The time step in the warped time system is chosen to be $\Delta\theta = 10^{-3}$.

If we focus on the periodic boundary condition employed, we may assume that the effects of diffusion in the Lagrangian frame are primarily focused on the region near the interface. Only when the reactive mixing scale becomes large enough to overlap with the reactive mixing scales of the products formed at the periodic ends, does the assumption that $z \to \pm\infty$, which signifies the semi-infinite domain as per the 1D analysis in the present work, begins to lose its validity. Our study focuses on the behavior of the system at times before the merging of the two fronts happens.

It appears clearly in figure B.11 that the temporal evolution of the mass of the product, m_c, obtained through the two aforementioned methods (the solution obtained through the 2D simulations in COMSOL Multiphysics is denoted by the symbols while that obtained from the 1D methodology is denoted by the solid

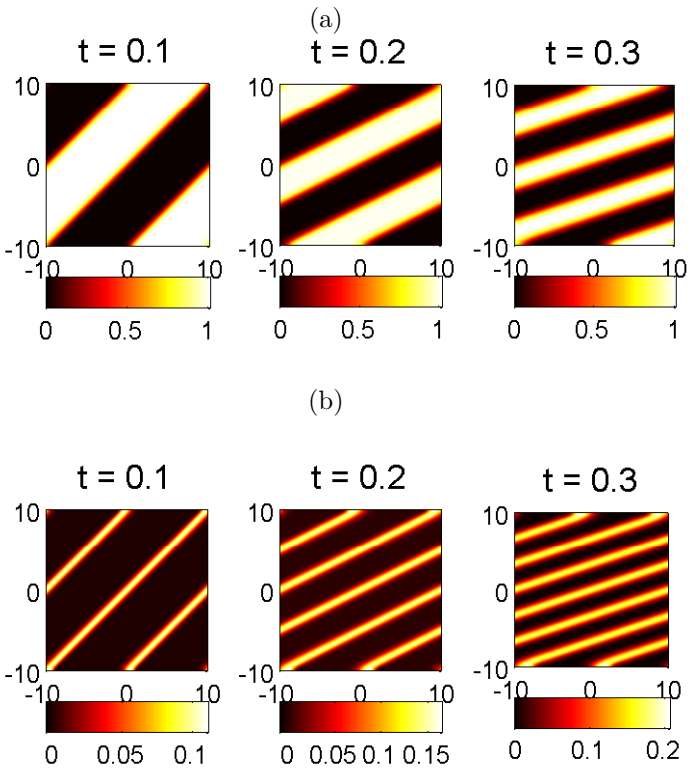

Figure B.12: (a) Surface plot of the reactant concentrations at different times during the 2D COMSOL simulation. We have chosen $\mathsf{Pe} = 10$ and $\mathsf{Da} = 10$ in this case. (b) Surface plot of the product concentration at different times during the 2D COMSOL simulation. We have chosen $\mathsf{Pe} = 10$ and $\mathsf{Da} = 10$ in this case.

lines) are in excellent agreement with each other for both the cases of $\mathsf{Da} = 10, \mathsf{Pe} = 1$ and $\mathsf{Da} = 0.1, \mathsf{Pe} = 10$.

In figure B.12 (a) and (b) we depict how the reactants and the products are stretched along the direction of the shear, leading to a corresponding compression in the perpendicular direction for times $t = 0.1, 0.2, 0.3$ for the case where $\mathsf{Pe} = 10$ and $\mathsf{Da} = 10$. As time progresses, the fronts from the other periodic cells start entering our cell of interest. Here at very large times, the fronts may come very close together so that the reactive mixing scales may overlap [65]. The product is formed at the interface between the two fronts and thus a larger number of bands can be observed for the surface plot of the product (figure B.12(b)).

In figure B.13, we depict the concentration distributions obtained from the COMSOL simulations in the direction normal to the interface, and compare them with those obtained from the 1D Chebyshev spectral collocation simulation. It is observed that for the case of small Péclet the number of peaks at $t = 0.35$ in the domain depicted in figure B.13 is only one while at a higher Péclet, we observe multiple peaks. It may be noted that so long as the concentration between the two peaks reaches zero, which implies independence of the two peaks, the results from the 1D simulation are valid. It may also be confirmed from figure B.13 that the concentration profiles predicted from the 1D Chebyshev spectral collocation method and full 2D simulation are in excellent agreement with each other. In the case of the 1D simulations, the boundary

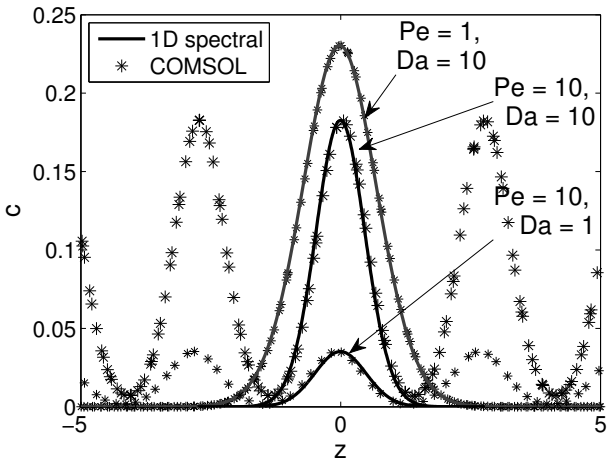

Figure B.13: Concentration profiles at $t = 0.35$, obtained in the direction perpendicular to the stretching interface from COMSOL 2D simulations and the 1D Chebyshev spectral collocation method. We depict the concentration profiles for 3 different cases $\mathsf{Pe} = 1, \mathsf{Da} = 10$, $\mathsf{Pe} = 10, \mathsf{Da} = 10$ and $\mathsf{Pe} = 10, \mathsf{Da} = 1$. The presence of multiple peaks in the figure from the 2D simulation is due to the fact that the periodicity employed for the 2D simulation causes the neighbouring fronts to enter the region of interest (this can be confirmed from the surface plots depicted in figure B.12).

condition that is implemented is in effect that of an infinite span of the domain in either directions. In the case of 2D simulations, we have taken into account the finite length of the reaction fronts. Given that the predictions of the methodology is applicable to a time before which the periodic fronts coalesce, the scenario of the two simulations are essentially the same. Hence the methodology elucidated in section 5 may be extended for complicated forms of the reactions with relative ease and with a high degree of accuracy.

Appendix C. Derivation of the dilution index for a conservative scalar

The dilution index is defined as

$$E(t) = \exp(S(t)) \tag{C.1}$$

where $S(t) = -\int d\mathbf{x}\, p(\mathbf{x},t) \ln p(\mathbf{x},t)$ represents the system entropy and $p(\mathbf{x},t)$ is the normalized concentration defined as $p(\mathbf{x},t) = c(\mathbf{x},t) / \int dx\, c(\mathbf{x},t)$ [79]. For a conservative scalar, the analytical solution for the concentration distribution is obtained as [54]

$$c = \frac{1}{(1+4\theta)} \exp\left(\frac{-x'^2}{\delta^2(1+4\theta)}\right). \tag{C.2}$$

Utilizing this solution, we obtain the normalized concentration and system entropy in the forms

$$\begin{aligned} p(\mathbf{x},t) &= \frac{e^{-\frac{x'^2}{\delta^2(1+4\theta)}}}{\sqrt{\pi}\sqrt{1+4\theta}\delta} \\ \text{and} \quad S(t) &= \frac{1}{2} + \frac{1}{2}\ln(1+4\theta) + \ln(\delta) + \frac{1}{2}\ln(\pi) \quad , \end{aligned} \tag{C.3}$$

respectively, where it is noted that the form of the stretching and warped time are as of now arbitrary. Utilizing the specific results for the linear stretching, we obtain

$$E = \exp\left[\frac{1}{2} + \frac{1}{2}\ln\left(1 + 4t + \frac{4}{3}t^3\mathsf{Pe}^2\right) - \frac{1}{2}\ln\left(1 + \mathsf{Pe}^2t^2\right) + \frac{1}{2}\ln\left(\pi\right)\right]. \tag{C.4}$$

In order to assess the behaviour of the derivative, we attempt to find the extremum (it is observed that the extremum is a minimum). Thus, $dE/dt = 0$ yields

$$\left(\frac{1}{2}\frac{4 + 4\mathsf{Pe}^2t^2}{1 + 4t + \frac{4}{3}t^3\mathsf{Pe}^2} - \frac{\mathsf{Pe}^2t}{1 + \mathsf{Pe}^2t^2}\right) e^{\frac{1}{2}+\frac{1}{2}\ln\left(1+4t+\frac{4}{3}t^3\mathsf{Pe}^2\right)-\frac{1}{2}\ln\left(1+\mathsf{Pe}^2t^2\right)+\frac{1}{2}\ln(\pi)} = 0 \tag{C.5}$$

which implies that $\left(\frac{1}{2}\frac{4+4\mathsf{Pe}^2t^2}{1+4t+\frac{4}{3}t^3\mathsf{Pe}^2} - \frac{\mathsf{Pe}^2t}{1+\mathsf{Pe}^2t^2}\right) = 0$. In the limit of $\mathsf{Pe}t \ll 1$, the aforementioned expression yields the corresponding time at which the minimum in dilution occurs to be, as $t = 1/\left(2^{1/3}\mathsf{Pe}^{2/3}\right)$, which is the same mixing time as that obtained in section 4.

References

[1] T. Tel, A. de Mourab, C. Grebogib, G. Károlyid, Chemical and biological activity in open flows: A dynamical system approach, Phys. Rep. 413 (2005) 91–196.

[2] A. Tartakovsky, G. Tartakovsky, T. Scheibe, Effects of incomplete mixing on multicomponent reactive transport, Advances in Water Resources 32 (11) (2009) 1674–1679.

[3] M. Dentz, T. Le Borgne, A. Englert, B. Bijeljic, Mixing, spreading and reaction in heterogeneous media: A brief review, Journal of Contaminant Hydrology 120-121 (2011) 1–17.

[4] M. W. Saaltink, V. Vilarrasa, F. De Gaspari, O. Silva, J. Carrera, T. S. Rötting, A method for incorporating equilibrium chemical reactions into multiphase flow models for CO2 storage, Advances in Water Resources 62 (2013) 431–441.

[5] X. Fu, L. Cueto-Felgueroso, D. Bolster, R. Juanes, Rock dissolution patterns and geochemical shutdown of co2-brine-carbonate reactions during convective mixing in porous media., J. of Fluid Mech. 726 (2015) 296–315.

[6] J. J. Hidalgo, M. Dentz, Y. Cabeza, J. Carrera, Dissolution patterns and mixing dynamics in unstable reactive flow, Geophys. Res. Lett. 42 (2015) 6357–6364.

[7] A. Ovchinnikov, Y. B. Zeldovich, Role of density fluctuations in bimolecular reaction kinetics, Chemical Physics 28 (1-2) (1978) 215–218.

[8] C. J. Werth, O. A. Cirpka, P. Grathwohl, Enhanced mixing and reaction through flow focusing in heterogeneous porous media, Water Resources Research 42 (12) (2006) W12414.

[9] X. Sanchez-Vila, M. Dentz, L. D. Donado, Transport-controlled reaction rates under local non-equilibrium conditions, Geophysical Research Letters 34 (10) (2007) L10404.

[10] M. De Simoni, X. Sanchez-Vila, J. Carrera, M. W. Saaltink, A mixing ratios-based formulation for multicomponent reactive transport, Water Resources Research 43 (7) (2007) W07419.

[11] M. Willmann, J. Carrera, X. Sanchez-Vila, O. Silva, M. Dentz, Coupling of mass transfer and reactive transport for non-linear reactions in heterogeneous media,, Water Resour. Res. (2010) W07512–W07526.

[12] O. A. Cirpka, A. J. Valocchi, Two-dimenstional concentration distribution for mixing-controlled bioreactive transport in steady-state, Adv. in Water Resour. 30 (2007) 1668–1679.

[13] G. Chiogna, D. Hochstetler, A. Bellin, P. Kitanidis, M. Rolle, Mixing, entropy and reactive solute transport., Geophys. Res. Lett. 39 (2012) L20405.

[14] D. L. Hochstettler, P. K. Kitanidis, The behavior of effective reaction rate constants for bimolecular reaction under physical equilibrium, J. Contam. Hydrol. 144 (2013) 88–98.

[15] H. Rajaram, L. W. Gelhar, Plume scale-dependent dispersion in heterogeneous aquifers: 1. lagrangian analysis in a stratified aquifer, Water Resources Research 29 (9) (1993) 3249–3260.

[16] O. A. Cirpka, F. P. J. de Barros, G. Chiogna, M. Rolle, W. Nowak, Stochastic flux-related analysis of transverse mixing in two-dimensional heterogeneous porous media, Water Resources Research 47 (6) (2011) W06515.

[17] M. Dentz, F. P. J. de Barros, Mixing-scale dependent dispersion for transport in heterogeneous flows, Journal of Fluid Mechanics 777 (2015) 178–195.

[18] X. Fu, L. Cueto-Felgueroso, D. Bolster, R. Juanes, Rock dissolution patterns and geochemical shutdown of–brine–carbonate reactions during convective mixing in porous media, Journal of Fluid Mechanics 764 (2015) 296–315.

[19] J. M. Ottino, W. E. Ranz, C. W. Macosko, A lamellar model for analysis of liquid-liquid mixing, Chemical Engineering Science 34 (6) (1979) 877–890.

[20] J.-j. Ou, W. Ranz, Mixing and chemical reactions, Chemical Engineering Science 38 (7) (1983) 1015–1019.

[21] M. D. Finn, J.-L. Thiffeault, Topological Optimization of Rod-Stirring Devices, SIAM Review 53 (4) (2011) 723–743.

[22] J. Weiss, A. Provenzale, Transport and Mixing in Geophysical Flows, no. 744, Springer Verlag, 2008.

[23] A. De Wit, Fingering of chemical fronts in porous media, Phys. Rev. Lett. 87 (2001) 054502.

[24] P. de Anna, J. Jimenez-Martinez, H. Tabuteau, R. Turuban, T. Le Borgne, M. Derrien, Y. Méheust, Mixing and Reaction Kinetics in Porous Media: An Experimental Pore Scale Quantification, Environmental Science & Technology 48 (1) (2014) 508–516.

[25] T. Le Borgne, T. R. Ginn, M. Dentz, Impact of fluid deformation on mixing-induced chemical reactions in heterogeneous flows, Geophysical Research Letters 41 (22) (2014) 7898–7906.

[26] L. Galfi, Z. Racz, Properties of the reaction front in an A+B-C type reaction-diffusion process, Phys. Rev. A 38 (6) (1988) 3151–3154.

[27] H. Larralde, M. Araujo, S. Havlin, H. E. Stanley, Reaction front for A + B $\rightarrow$ C diffusion-reaction systems with initially separated reactants, Physical Review A 46 (2) (1992) 855–859.

[28] H. Taitelbaum, S. Havlin, J. E. Kiefer, B. Trus, G. H. Weiss, Some properties of the a+b $\rightarrow$ C reaction-diffusion system with initially separated components, Journal of Statistical Physics 65 (5-6) (1991) 873–891.

[29] M. Arshadi, H. Rajaram, A transition in the spatially integrated reaction rate of bimolecular reaction-diffusion systems, Water Resources Research 51 (2015) 7798–7810.

[30] B. Chopard, M. Droz, T. Karapiperis, Z. Rácz, Properties of the reaction front in a reversible A + B $\rightleftharpoons$ C reaction-diffusion process, Physical Review E 47 (1) (1993) R40–R43.

[31] M. Sinder, J. Pelleg, Asymptotic properties of a reversible a+ b c (static) reaction-diffusion process with initially separated reactants, Physical Review E 62 (3) (2000) 3340.

[32] S. J. Cornell, Refined simulations of the reaction front for diffusion-limited two-species annihilation in one dimension, Physical Review E 51 (5) (1995) 4055.

[33] M. Howard, J. Cardy, Fluctuation effects and multiscaling of the reaction-diffusion front for a+ b to oe, Journal of Physics A: Mathematical and General 28 (13) (1995) 3599.

[34] J. H. Merkin, D. J. Needham, Propagating reaction-diffusion waves in a simple isothermal quadratic autocatalytic chemical system, Journal of Engineering Mathematics 23 (4) (1989) 343–356.

[35] J. Merkin, D. Needham, S. Scott, The development of travelling waves in a simple isothermal chemical system i. quadratic autocatalysis with linear decay, in: Proceedings of the Royal Society of London A: Mathematical, Physical and Engineering Sciences, Vol. 424, The Royal Society, 1989, pp. 187–209.

[36] J. Merkin, D. Needham, The development of travelling waves in a simple isothermal chemical system ii. cubic autocatalysis

with quadratic and linear decay, in: Proceedings of the Royal Society of London A: Mathematical, Physical and Engineering Sciences, Vol. 430, The Royal Society, 1990, pp. 315–345.

[37] P. Gray, J. Merkin, D. Needham, S. Scott, The development of travelling waves in a simple isothermal chemical system iii. cubic and mixed autocatalysis, in: Proceedings of the Royal Society of London A: Mathematical, Physical and Engineering Sciences, Vol. 430, The Royal Society, 1990, pp. 509–524.

[38] H. Taitelbaum, Segregation in reaction-diffusion systems, Physica A: Statistical Mechanics and its Applications 200 (1) (1993) 155–164.

[39] H. Taitelbaum, A. Yen, R. Kopelman, S. Havlin, G. H. Weiss, Effects of bias on the kinetics of a+ b c with initially separated reactants, Physical Review E 54 (6) (1996) 5942.

[40] Y.-E. L. Koo, R. Kopelman, Space-and time-resolved diffusion-limited binary reaction kinetics in capillaries: experimental observation of segregation, anomalous exponents, and depletion zone, Journal of Statistical Physics 65 (5-6) (1991) 893–918.

[41] S. H. Park, S. Parus, R. Kopelman, H. Taitelbaum, Gel-free experiments of reaction-diffusion front kinetics, Physical Review E 64 (5) (2001) 055102.

[42] S. Havlin, M. Araujo, H. Larralde, A. Shehter, H. Stanley, Anomalous kinetics in A + B $\rightarrow$ C with initially-separated reactants, Chaos, Solitons & Fractals 6 (94) (1995) 157–169.

[43] M. Z. Bazant, H. Stone, Asymptotics of reaction-diffusion fronts with one static and one diffusing reactant, Physica D: Nonlinear Phenomena 147 (1-2) (2000) 95–121.

[44] H. Taitelbaum, Z. Koza, Anomalous kinetics of reaction diffusion fronts, Philosophical Magazine Part B 77 (5) (1998) 1389–1400.

[45] Z. Koza, The long-time behavior of initially separated a+ b 0 reaction-diffusion systems with arbitrary diffusion constants, Journal of statistical physics 85 (1-2) (1996) 179–191.

[46] P. Polanowski, Z. Koza, Reaction-diffusion fronts in systems with concentration-dependent diffusivities, Physical Review E 74 (3) (2006) 036103.

[47] D. A. Benson, D. Bolster, A. Paster, Communication: A full solution of the annihilation reaction a + b $\rightarrow \phi$ based on time-subordination, The Journal of Chemical Physics 138 (13).

[48] M. Sinder, V. Sokolovsky, J. Pelleg, Reversible a $\leftrightarrow$ b reaction–diffusion process with initially mixed reactants: Boundary layer function approach, Physica B: Condensed Matter 406 (15) (2011) 3042–3049.

[49] M. Sinder, J. Pelleg, Two reaction zones in a competing reactions system with initially separated components, Physical Review E 65 (6) (2002) 060101.

[50] C. J. Allègre, D. L. Turcotte, Implications of a two-component marble-cake mantle, Nature 323 (6084) (1986) 123–127.

[51] P. B. Rhines, W. R. Young, How rapidly is a passive scalar mixed within closed streamlines?, Journal of Fluid Mechanics 133 (1983) 133.

[52] E. Villermaux, H. Rehab, Mixing in coaxial jets, Journal of Fluid Mechanics 425 (2000) 161–185.

[53] Z. Neufeld, E. Hernández-García, Chemical and biological processes in fluid flows, World Scientific, 2009.

[54] P. Meunier, E. Villermaux, The diffusive strip method for scalar mixing in two dimensions, Journal of Fluid Mechanics 662 (2010) 134–172.

[55] J. M. Ottino, The kinematics of mixing: stretching, chaos, and transport, Vol. 3, Cambridge university press, 1989.

[56] W. E. Ranz, Applications of a stretch model to mixing, diffusion, and reaction in laminar and turbulent flows, AIChE Journal 25 (1) (1979) 41–47.

[57] M. J. Clifford, A Gaussian model for reaction and diffusion in a lamellar structures, Chem. Eng. J. 54 (1999) 303–310.

[58] M. J. Clifford, S. M. Cox, E. P. L. Roberts, Lamellar modelling of reaction, diffusion and mixing in a two-dimensional flow, Chem. Eng. Sci. 71 (1998) 49–56.

[59] A. Paster, T. Aquino, D. Bolster, Incomplete mixing and reactions in a laminar shear flow, Phys. Rev. E 92 (2015) 012922.

[60] E. Villermaux, Mixing by porous media, Comptes Rendus - Mecanique 340 (11-12) (2012) 933–943.

[61] I. Battiato, D. Tartakovsky, A. Tartakovsky, T. Scheibe, On breakdown of macroscopic models of mixing-controlled heterogeneous reactions in porous media, Advances in Water Resources 32 (11) (2009) 1664 – 1673.

[62] I. Battiato, D. M. Tartakovsky, A. M. Tartakovsky, T. D. Scheibe, Hybrid models of reactive transport in porous and fractured media, Advances in Water Resources 34 (9) (2011) 1140–1150.

[63] F. Boso, I. Battiato, Homogenizability conditions for multicomponent reactive transport, Advances in Water Resources 62 (2013) 254–265.

[64] J. D. Hyman, P. K. Smolarkiewicz, C. L. Winter, Heterogeneities of flow in stochastically generated porous media, Physical Review E 86 (5) (2012) 056701.

[65] T. Le Borgne, M. Dentz, E. Villermaux, Stretching, Coalescence, and Mixing in Porous Media, Physical Review Letters 110 (20) (2013) 204501.

[66] T. Le Borgne, M. Dentz, E. Villermaux, The lamellar description of mixing in porous media, Journal of Fluid Mechanics 770 (2015) 458–498.

[67] M. Rolle, P. K. Kitanidis, Effects of compound-specific dilution on transient transport and solute breakthrough: A pore-scale analysis, Advances in Water Resources 71 (2014) 186–199.

[68] D. Bolster, A. Paster, D. A. Benson, A particle number conserving Lagrangian method for mixing-driven reactive transport, Water Resources Research 52 (2016) 1518–1527.

[69] D. C. Mays, R. M. Neupauer, Plume spreading in groundwater by stretching and folding, Water Resources Research 48 (7) (2012) W07501.

[70] C. M. Gramling, C. F. Harvey, L. C. Meigs, Reactive Transport in Porous Media: A Comparison of Model Prediction with Laboratory Visualization, Environmental Science & Technology 36 (11) (2002) 2508–2514.

[71] J. Jiménez-Martínez, P. de Anna, H. Tabuteau, R. Turuban, T. L. Borgne, Y. Méheust, Pore-scale mechanisms for the enhancement of mixing in unsaturated porous media and implications for chemical reactions, Geophysical Research Letters 42 (13) (2015) 5316–5324.

[72] P. Oates, Upscaling reactive transport in porous media: laboratory visualization and stochastic models, Ph.D. thesis, Mass. Inst. Technol., USA (2007).

[73] G. Chiogna, A. Bellin, Analytical solution for reactive solute transport considering incomplete mixing within a reference elementary volume, Water Resources Research 49 (5) (2013) 2589–2600.

[74] G. Matheron, G. De Marsily, Is transport in porous media always diffusive? a counterexample, Water Resources Research 16 (5) (1980) 901–917.

[75] D. Bolster, F. J. Valdés-Parada, T. LeBorgne, M. Dentz, J. Carrera, Mixing in confined stratified aquifers, Journal of contaminant hydrology 120 (2011) 198–212.

[76] A. Fiori, G. Dagan, Transport of a passive scalar in a stratified porous medium, Transport in porous media 47 (1) (2002) 81–98.

[77] S. W. Weeks, G. Sposito, Mixing and stretching efficiency in steady and unsteady groundwater flows, Water resources research 34 (12) (1998) 3315–3322.

[78] M. Dentz, J. Carrera, Mixing and spreading in stratified flow, Physics of Fluids (1994-present) 19 (1) (2007) 017107.

[79] F. P. Barros, M. Dentz, J. Koch, W. Nowak, Flow topology and scalar mixing in spatially heterogeneous flow fields, Geophysical Research Letters 39 (8) (2012) L08404.

[80] D. R. Lester, M. Dentz, T. Le Borgne, Chaotic mixing in three-dimensional porous media, J. of Fluid Mech. 803 (2016) 144–174.

[81] P. de Anna, M. Dentz, A. Tartakovsky, T. Le Borgne, The filamentary structure of mixing fronts and its control on reaction

kinetics in porous media flows, Geophys. Res. Lett. 41 (2014) 4586–4593.

[82] C. I. Steefel, D. J. DePaolo, P. C. Lichtner, Reactive transport modeling: An essential tool and a new research approach for the earth sciences, Earth and Planetary Science Letters 240 (3) (2005) 539–558.

[83] C. A. J. Appelo, D. Postma, Geochemistry, groundwater and pollution, CRC press, 2004.

[84] K. Maher, C. Chamberlain, Hydrologic regulation of chemical weathering and the geologic carbon cycle, Science 343 (6178) (2014) 1502–1504.

[85] J. Crank, The Mathematics of Diffusion, second edi Edition, Oxford University Press, New York, 1975.

[86] F. Incropera, D. DeWitt, Introduction to heat transfer, Wiley, 1985.

[87] P. Kundu, I. Cohen, H. Hu, Fluid Mechanics, sixth edition Edition, Academic Press, New Delhi, 2012.

[88] M. Alvarez, F. Muzzio, S. Cerbelli, A. Adrover, M. Giona, Self-similar spatiotemporal structure of intermaterial boundaries in chaotic flows, Physical review letters 81 (16) (1998) 3395.

[89] S. Cerbelli, M. Alvarez, F. Muzzio, Prediction and quantification of micromixing intensities in laminar flows, AIChE journal 48 (4) (2002) 686–700.

[90] E. Hernández-Garcia, C. López, Sustained plankton blooms under open chaotic flows, Ecological Complexity 1 (3) (2004) 253–259.

[91] T. Le Borgne, M. Dentz, P. Davy, D. Bolster, J. Carrera, J.-R. de Dreuzy, O. Bour, Persistence of incomplete mixing: A key to anomalous transport, Phys. Rev. E 84 (2011) 015301(R).

[92] L. N. Trefethen, Spectral Methods in MATLAB, Society for Industrial and Applied Mathematics, 2000.

[93] M. Dentz, D. R. Lester, T. L. Borgne, F. P. de Barros, Fluid stretching as a lévy process, arXiv preprint arXiv:1602.04904.